

Review

# Recent Advances in Rational Design and Engineering of Signal-Amplifying Substrates for Surface-Enhanced Raman Scattering-Based Bioassays

Song Gao, Zhanchen Guo  and Zhen Liu \* 

State Key Laboratory of Analytical Chemistry for Life Science, School of Chemistry and Chemical Engineering, Nanjing University, Nanjing 210023, China; song.gao@smail.nju.edu.cn (S.G.); zcguo@smail.nju.edu.cn (Z.G.)

\* Correspondence: zhenliu@nju.edu.cn

**Abstract:** In recent decades, surface-enhanced Raman spectroscopy (SERS) has become a powerful detection scheme for many applications, particularly bioassays, due to its unique strengths, such as its ultrasensitive performance. Due to the development of various SERS substrates, more SERS-based bioassays with improved sensitivity and reproducibility have been designed and manufactured. SERS is able to provide the intrinsic vibration information of molecules through the unique Raman fingerprint to enable direct detection and quantitation. Meanwhile, with the assistance of Raman-active labels, biomolecules, like proteins and nucleic acids, can be detected by the immunosandwich assay. In this review, we focus on the rational design and engineering of signal-enhancing substrates for SERS-based bioassays. Those substrates are classified into two categories, i.e., nanoparticles in colloidal suspension and nanostructures on a solid support. Each category is discussed in detail with stress on their biomedical application potential. Afterward, we summarize the SERS-based assays of proteins, nucleic acids, and viruses, for which both label-free and labeled approaches play important roles. Finally, we present the remaining challenges in the field of SERS-based bioassays and sketch out promising directions for future development.



**Citation:** Gao, S.; Guo, Z.; Liu, Z. Recent Advances in Rational Design and Engineering of Signal-Amplifying Substrates for Surface-Enhanced Raman Scattering-Based Bioassays. *Chemosensors* **2023**, *11*, 461. <https://doi.org/10.3390/chemosensors11080461>

Academic Editor: Rui Martins

Received: 25 July 2023

Revised: 10 August 2023

Accepted: 13 August 2023

Published: 16 August 2023



**Copyright:** © 2023 by the authors. Licensee MDPI, Basel, Switzerland. This article is an open access article distributed under the terms and conditions of the Creative Commons Attribution (CC BY) license (<https://creativecommons.org/licenses/by/4.0/>).

**Keywords:** Raman spectroscopy; SERS substrate; rational design; bioassays; high-sensitivity analysis

## 1. Introduction

Surface-enhanced Raman scattering (SERS) has emerged as a powerful analytical technique across many application domains. It combines Raman spectroscopy with nanostructured metal surfaces to achieve significant enhancement of the Raman signal. The conventional Raman spectroscopy, discovered by Raman and Krishnan in 1928 [1], has served as an analytical tool for a wide range of applications. Raman scattering provides insights into molecular structures by revealing their vibrational spectra. It provides compound-specific information and molecular-level fingerprinting without the need for complex instruments. This characteristic makes it promising for sensing various analyte molecules, and it has found extensive use in biological applications [2–5]. For example, it has been employed in identifying cancer cells [6], investigating biomolecular structures [7], and diagnosing diseases and pathologies [8,9]. Despite its utility, Raman scattering intensity is typically weak, as the process suffers from low efficiency. Upon light-matter interactions, only one in every  $10^8$  photons would undergo an inelastic scattering as estimated [10,11]. This limitation has hindered its application in trace analysis, necessitating methods to enhance the Raman signal. Fortunately, Fleischmann, Hendra, and McQuilian first observed unexpectedly strong Raman signals in 1974 from pyridine adsorbed on roughened silver electrodes [12]. Later, in 1977, Jeanmaire and Van Duyne discovered that placing a Raman-active species on a roughened noble metal surface significantly amplified the Raman signal, surpassing the limitations of conventional Raman scattering [13]. This phenomenon, known as surface-enhanced Raman scattering, has revolutionized the sensitivity of Raman

spectroscopy. Now SERS is one of the key technologies to dramatically amplify the Raman scattering signal in order to bring several advantages, including ultrahigh sensitivity, less susceptibility to sample environment, rapid readout speed, and the possibility of on-site or field detection [14].

Bioassays are crucial tools in biological and pharmaceutical research, providing valuable information about the role and effects of substances in living organisms. They facilitate the evaluation of biological activity [15], assist early disease diagnostics [16], aid in drug discovery and development [17], ensure quality control [18], assess toxicity [19], monitor environmental impact [20], and contribute to expanding our understanding of living systems [21]. Both labeled and label-free bioassays have gained prominence as powerful tools for studying and analyzing biological systems. Labeled bioassays involve the use of molecular probes or labels, such as fluorescent dyes and radioisotopes, to detect and quantify the biomolecules of interest that have been specifically captured. These labels enable the direct measurement and visualization of the target, providing specific and sensitive results. Label-free bioassays, on the other hand, rely on the direct measurement of intrinsic properties of the captured biomolecule, such as mass, absorbance, and Raman response, without the use of exogenous labels. In general, labeled assays provide high sensitivity and versatility, but require sample manipulation and may introduce biases. Conversely, label-free assays offer minimal sample processing and real-time analysis but may lack sensitivity and pose challenges in data interpretation. As technology continues to advance, the development of hybrid strategies and improved detection methods may bridge the gap between these two bioassay paradigms, enabling researchers to harness the strengths of both approaches in their scientific investigations.

Conventional bioassays mainly rely on the use of absorbance, fluorescence, and chemiluminescence for detection. However, SERS-based bioassays have garnered significant interest in recent decades due to the unique advantages over these detection schemes. One of the primary advantages is suitability for multiplexing [22]. Raman bands in SERS have narrower widths as compared with fluorescence, enabling simultaneous measurement of multiple analytes within a single detection. Another advantage is the high enhancement factor (EF) in SERS, which ranges from  $10^6$  to  $10^{14}$  [23–25], making SERS an exceptionally sensitive tool. The high sensitivity of SERS is particularly favorable for the detection of low-abundance substances of biological importance in complex real samples. By combining the specific binding capabilities of antibodies with the enhanced sensitivity of SERS, SERS-based bioassays provide a powerful tool for the detection and quantification of target analytes.

Raman signal-enhancing substrates play a vital role in SERS, enabling ultrasensitive detection and characterization of biological analytes. The rational design of SERS substrates involves tailoring their properties at the nanoscale to optimize the enhancement factor and ensure high reproducibility. Since there have been numerous publications devoted to the design and fabrication of substrates for SERS measurement, several review papers have well-surveyed the advances in this area [26–30]. A critical review is still needed on the progress of SERS-based bioassays, particularly from the view of the exquisite design, performance improvement, and real-world application potential.

In this review, we survey recent advances in SERS-based bioassays with a focus on the rational design and engineering of signal-enhancing substrates. For convenience of comparison and understanding, we classify the substrates into two categories, i.e., nanoparticles in colloidal suspension and nanostructures on a solid support. Each category is discussed in detail with stress on their biomedical application potential. SERS-based bioassays have been applied to various clinical samples. We further summarize the SERS-based assays of proteins, nucleic acids, and viruses, for which both label-free and labeled approaches play important roles. Finally, we suggest other challenges in the field of SERS-based bioassays and sketch out promising directions for future development.

## 2. Basic Theory of SERS

It is now generally accepted that the Raman scattering signal is amplified through a combination of electromagnetic (EM) enhancement mechanism, and chemical (CM) enhancement mechanism. In brief, electromagnetic enhancement arises from the excitation of localized surface plasmons, which are collective oscillations of conduction electrons on the metal surface. These plasmons generate intense electromagnetic fields at the metal surface, leading to increased Raman scattering intensity. The chemical enhancement, on the other hand, results from the charge transfer between the molecule and the metal surface, further enhancing the Raman signal. Chemical enhancement is highly dependent on the specific molecule–substrate interactions and can vary for different analytes.

### 2.1. Electromagnetic Enhancement

The underlying principle of SERS involves the amplification of the incident and scattered electromagnetic fields when a nanostructured surface of the metal is irradiated with the frequency of localized surface plasmons resonance (LSPR) on the metal surface. This phenomenon is explained by considering a metal nanosphere subjected to an external electric field (Figure 1A). The oscillating electric field ( $E_0$ ) of the incident light interacts with the metal nanoparticle, inducing a polarization of charge and creating a dipolar localized surface plasmon resonance. This polarization generates an induced dipole moment ( $\mu_{\text{ind}}$ ) determined by the metal polarizability ( $\alpha_{\text{met}}$ ) and the incident electric field ( $E_0(\omega_{\text{inc}})$ ) [31].

$$\mu_{\text{ind}} = \alpha_{\text{met}} E_0(\omega_{\text{inc}}) \quad (1)$$

As a Raman scattering arises on a molecule, a dipole moment is first created by the incident light. After being scattered, the photons are detected as the Raman signal. SERS follows a similar process but with the enhancement of the local electromagnetic field due to hotspots on the metal surface. In SERS, the inelastic scattering of  $E_0$  generates an enhanced local electric field ( $E_{\text{loc}}$ ) near the metal surface. The interaction between the local electric field and the molecule adsorbed on the surface creates an induced dipole moment ( $\mu_{\text{ind}}$ ) determined by the molecular polarizability ( $\alpha_{\text{mol}}$ ) and the enhanced local electric field ( $E_{\text{loc}}(\omega_{\text{inc}})$ ).

$$\mu_{\text{ind}} = \alpha_{\text{mol}} E_{\text{loc}}(\omega_{\text{inc}}) \quad (2)$$

According to the vibrational spectrum theory in quantum mechanics, the presence of inelastic scattering for a vibrating molecule is explained by the incident electric field ( $E_{\text{inc}}$ ) and the eigenvalue of angular frequency ( $\omega_{\text{vib}}$ ) of the vibrating molecule. This inelastic scattering gives rise to three dipole components: Rayleigh scattering  $\mu_{\text{ind}}(\omega_{\text{inc}})$ , Stokes scattering  $\mu_{\text{ind}}(\omega_{\text{inc}} - \omega_{\text{vib}})$ , and anti-Stokes scattering  $\mu_{\text{ind}}(\omega_{\text{inc}} + \omega_{\text{vib}})$  (Figure 1B). The resonance frequency of surface plasmons on the metal surface determines the enhancement of the scattered Stokes field. Taking into account the incident and scattered field intensities, the overall SERS enhancement intensity can be described by an equation that involves the local electric field ( $E_{\text{inc}}(\omega_{\text{inc}})$ ) at the incident frequency ( $\omega_{\text{inc}}$ ) and the electric field ( $E(\omega_s)$ ) at the Stokes-shifted frequency ( $\omega_s = \omega_{\text{inc}} - \omega_{\text{vib}}$ ) [31].

$$I_{\text{SERS}} = I_{\text{inc}}(\omega_{\text{inc}}) I(\omega_s) \quad (3)$$

$$= |E_{\text{inc}}(\omega_{\text{inc}})|^2 |E(\omega_s)|^2 \quad (4)$$

When the electric field values at the incident frequency ( $E_{\text{inc}}(\omega_{\text{inc}})$ ) and the Stokes shifted frequency ( $E(\omega_s)$ ) are in proximity, the resulting enhancement derived from the electromagnetic mechanism follows the relationship where the SERS enhancement factor is directly proportional to the fourth power of the induced electric field enhancement value ( $E(\omega_{\text{inc}})$ ).

$$I_{\text{SERS}} = |E(\omega_{\text{inc}})|^4 \quad (5)$$

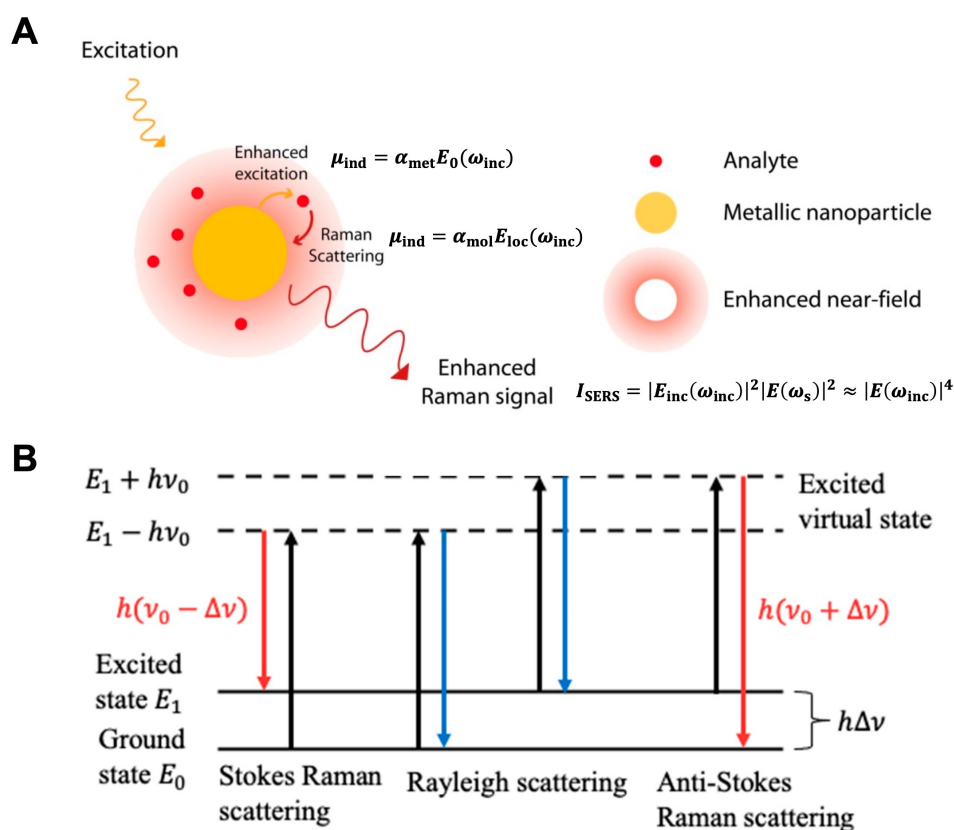


**Figure 1.** (A) Principal of surface-enhanced Raman scattering (reproduced under the terms of CC BY 4.0 from Ref. [32], copyright 2015, the authors). (B) Rayleigh scattering and Raman scattering energy-level diagram (reproduced under the terms of CC BY 4.0 from Ref. [33], copyright 2022, the authors).

## 2.2. Chemical Enhancement

The chemical effect is another significant mechanism contributing to SERS enhancement, and it requires direct contact between the SERS substrate and the analyte. This effect involves the interaction of the adsorbate and the surface to form a complex through electronic coupling. During this interaction, electrons on the substrate surface transfer from the Fermi level to the lowest unoccupied molecular orbital of the analyte molecule. This process leads to the creation of charge transfer intermediates, which demonstrate higher Raman cross-sections in comparison to the free molecule. If the incident photon at frequency  $\omega_{\text{inc}}$  resonates with the charge transfer transition of the formed complex, the scattered Stokes intensity contains information about the vibrational state of the molecule. In other words, the Raman spectrum of the analyte molecule is enhanced when it forms a chemical bond or interacts strongly with the SERS-active metal surface.

The magnitude of the chemical enhancement effect is typically in the range of  $10^0$  to  $10^2$ , which is weaker compared to the electromagnetic enhancement. However, the chemical effect can provide additional information about the chemical interactions between the analyte molecule and the metal surface, allowing for a more detailed characterization of the molecular species.

## 3. Substrates in Colloidal Suspension

SERS substrates designed for practical applications and problem-solving purposes have been extensively explored. These substrates in colloids can be broadly categorized into two groups: dispersed particles and aggregated systems. Dispersed particle systems in solution are relatively simple to prepare, making them widely used. Furthermore, advancements in producing increasingly uniform particles have improved the reproducibility

of SERS measurements. Surface functionalization of colloidal particles is also often straightforward, allowing for a wide range of targets and applications [34–36]. However, these systems suffer from some drawbacks, with colloidal stability being a primary concern, as colloidal systems tend to be unstable and prone to irreversible aggregation, particularly in complex environments.

Highly enhancing SERS substrates often consist of aggregated or assembled nanoparticles. While yielding significant SERS enhancement factors, reproducibility can sometimes be challenging due to the difficulty in controlling aggregation. Controlled particle assembly offers a solution to this issue, allowing for precise nanoengineering and reducing the irreproducibility associated with aggregated particles. The outcome of the assembly process is influenced by surface functionalization and nanoparticle geometry.

### 3.1. Dispersed Particles

With the advancements in nanoscience and nanotechnology, the synthesis of metal nanoparticles (with precise control over their sizes, shapes, and structures) has been widely explored. Numerous synthesis methods have been developed to create increasingly intricate nanostructures, including nanospheres [37], nanostars [38–40], nanotriangles [41], nanorods [42–44], nanocubes [34,45–47], core–shell particles [48,49], and others (Figure 2A). Higher order structures in SERS allow for increased control over regions with high field enhancement and enable optimization of plasmon modes for specific experiments. Chemical reduction methods have been used to achieve uniform structural control of nanoparticles. For example, using the seed-mediated growth method, gold nanospheres with successive and tunable diameters can be prepared, bringing size-dependent SERS properties [37,50].

Surfactants play a crucial role in the conventional synthesis process of nanoparticles, and the development of new types of surfactants can enable simplified and controllable synthetic methods for nanostructures, expanding their applications. Zhang et al. involved the natural compound epigallocatechin gallate (EGCG) as a reducing agent to synthesize different morphologies of gold nanoparticles (AuNPs) by changing the solution pH values [51]. The addition of halogen ions not only alleviates laser damage to nanoparticles but also promote the formation of a 3D hotspot, leading to a noticeable SERS effect that brings about high reproducibility and stability. In another study, bromide ions were introduced to induce anisotropic growth when synthesizing gold nanocubes (AuNCs) [45]. As bromide ions favorably adsorb onto the (100) facet, in combination with cetyltrimethylammonium chloride (CTAC), a difference in the accessibility of gold precursors to different facets is made, leading to distinct growth rates between [100] and other facets. At low bromide densities, the adsorbed bromide ions do not completely block the (100) facet, producing AuNCs with round corners. However, when an adequate amount of facet-directing agents is provided, preferential binding to the (100) facet maximizes the growth-rate difference between the (100) facet and the other two facets, resulting in AuNCs with sharp corners (Figure 2B). This straightforward and generally applicable synthetic strategy enables the precise control of the size and corner sharpness of gold nanocubes in a high yield. Similarly, iodide ions are used in the synthesis of gold nanotriangles [41]. Highly symmetric gold nanostars are enclosed by high-index facets to grow the hexagonal pyramidal arms, which are regulated by alkyl amines, like dimethylamine (DMA), methylamine, ethylamine, butylamine, and octylamine as shape-control agents [38]. Due to their high symmetry, Au nanostars demonstrate superior single-particle SERS performance in terms of both intensity and reproducibility when compared to asymmetric Au nanostars. In addition to chemical methods, laser-induced morphological remodeling of gold nanorods has been achieved by regulating the intensity of illumination and density of surfactant, resulting in different aspect ratios and ultranarrow local surface plasmon resonance bands [43]. This laser-controlled method enables the synthesis of gold nanorods with an ultranarrow LSPR band.

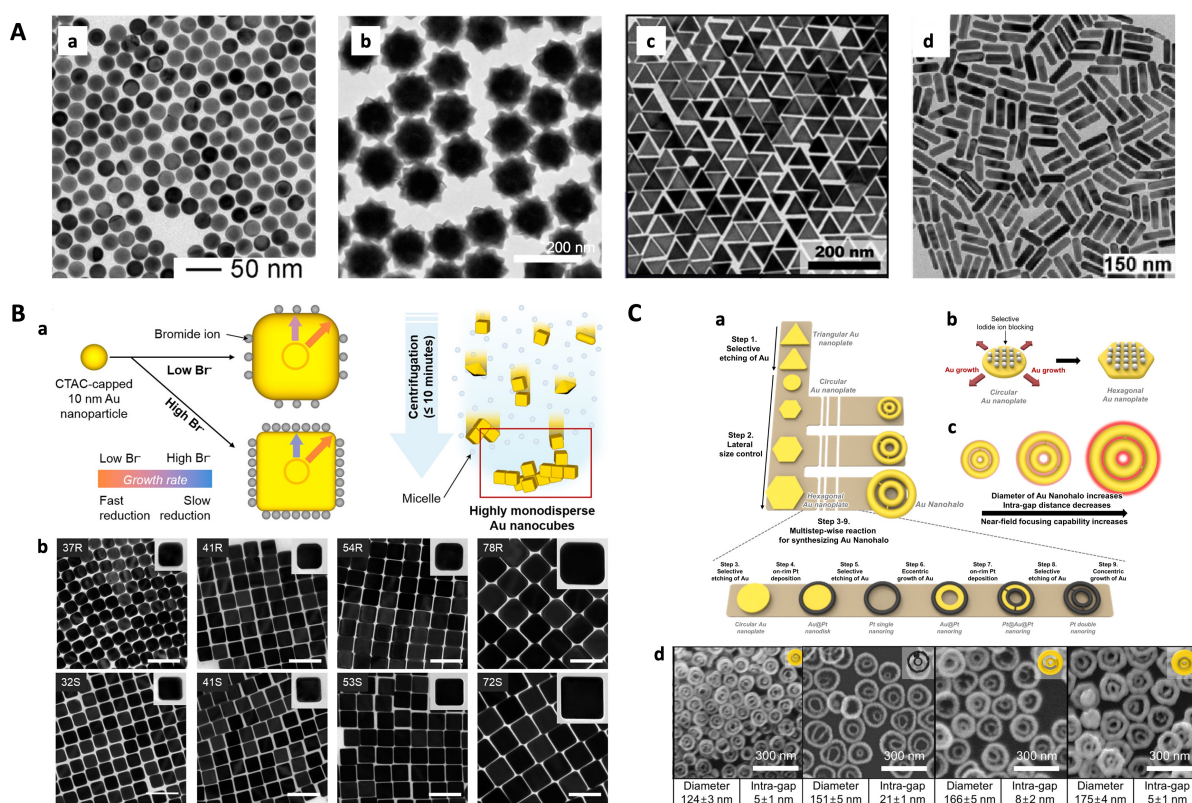


**Figure 2.** Representative substrates of dispersed nanoparticles in colloidal suspension. (A) Transmission electron microscope (TEM) images of controllable gold nanoparticles with different shapes: (a) nanospheres (reproduced with permission from Ref. [37], copyright 2013, WILEY-VCH Verlag GmbH & Co. KGaA, Weinheim, Germany), (b) nanostars (reproduced with permission from Ref. [38], copyright 2015, American Chemical Society), (c) nanotriangles (reproduced with permission from Ref. [41], copyright 2021, American Chemical Society), (d) nanorods (reproduced with permission from Ref. [42], copyright 2019, American Chemical Society). (B) (a) Schematic illustration representing the synthesis of corner-sharpness-controlled AuNCs with varied bromide densities followed by refinement by centrifugation-driven depletion-induced flocculation in surfactant micelle solutions; (b) TEM images of different sizes of round-cornered (R) and sharp-cornered (S) AuNCs (reproduced with permission from Ref. [45], copyright 2018, American Chemical Society). (C) (a) Schematic illustration representing the synthetic pathway of size-controlled Au nanohalos (Au double nanorings), including selective etching of Au, lateral size control, on-rim Pt deposition, selective etching of Au, eccentric growth of Au, and concentric growth of Au; (b) iodide ions blocking the top and bottom flat facets of circular Au nanoplates allow us to obtain diameter-controlled hexagonal Au nanoplates during the lateral size control step; (c) near-field focusing capability of Au nanohalos varies as a function of the diameter and intragap distance of Au nanohalos; (d) TEM images of Au nanohalos with different diameters and intra-gaps (reproduced with permission from Ref. [52], copyright 2022, American Chemical Society).

To achieve maximum near-field focusing around nanoscale metal particles, more complicated morphologies like gold double nanorings have been developed (Figure 2C) [52]. These nanorings consist of two concentric rings with nanoscale gaps between them. The circular intra-nanogaps create hot halos, enabling single-particle SERS when analytes are present within these gaps. The synthesis of Au nanohalos is based on a novel strategy utilizing hexagonal Au nanoplates as a template. By controlling the ratio of Au ions to iodide ions while maintaining the thickness, the lateral size of the nanoplates can be precisely controlled. Through multiple sequential steps, the initially triangular Au nanoplates are transformed into Au nanohalos with near-field focusing capabilities. The estimated enhancement factor achieved by these structures is remarkably high, ranging from  $1.1 \times 10^9$  to  $3.6 \times 10^9$ , and the results are highly reproducible. Another approach involves the evolu-

tion of chirality by adding chiral molecules during the synthesis, promoting asymmetric growth and inducing the chiroptical response of nanostructures [53]. This method allows for the preparation of single plasmonic gold nanoparticles with a significant uniform chiral gap, aiding in precise morphology and property control for chiral nanomaterials.

Overall, these advancements in the synthesis of reproducible nanostructures using various methods, including chemical reduction, surfactant-assisted fabrication, laser control, and chiral shape modifiers, offer opportunities for precise control over the morphology and optical properties of nanoparticles. These advances have implications for a wide range of applications, including SERS-based detection, where reproducibility, sensitivity, and reliability are critical.

### 3.2. Coupling of Particles

Multimeric nanostructures, such as dimers and trimers, provide inter-nanogap structures containing hotspots that exhibit intense electromagnetic field enhancement between adjacent particles. These hotspots are responsible for the extraordinary enhancement of Raman signals in SERS. He et al. introduced a dual biomimetic recognition-driven plasmonic nanogap-enhanced Raman scattering (DBR-PNERS) strategy for highly sensitive protein fingerprinting and quantification [54] (Figure 3A). This approach utilizes a pair of protein terminal epitope-imprinted plasmonic nanoantennas (PNAs) designed to bind to the N- and C-terminals of the target protein. An ultrathin imprinting layer (approximately 5 nm) is engineered on the PNAs, preserving the plasmonic signal enhancement effect of the nanoantennas and overcoming the limitations of larger antibodies. When both PNAs are present in a sample containing the target protein, specific binding occurs, forming a nanogap where the target protein is located. This nanogap provides a well-defined hot spot for Raman signal amplification, enabling precise molecular information readout and quantification of the target protein. Additionally, an internal standard (IS), in the form of a Raman-active small molecule, was incorporated into the nanoantenna, enabling a ratiometric assay for accurate and reliable quantification. Compared to existing approaches, DBR-PNERS exhibited several significant merits, including fingerprinting, robust quantitation, ultrahigh sensitivity, minimal sample consumption, and so on.

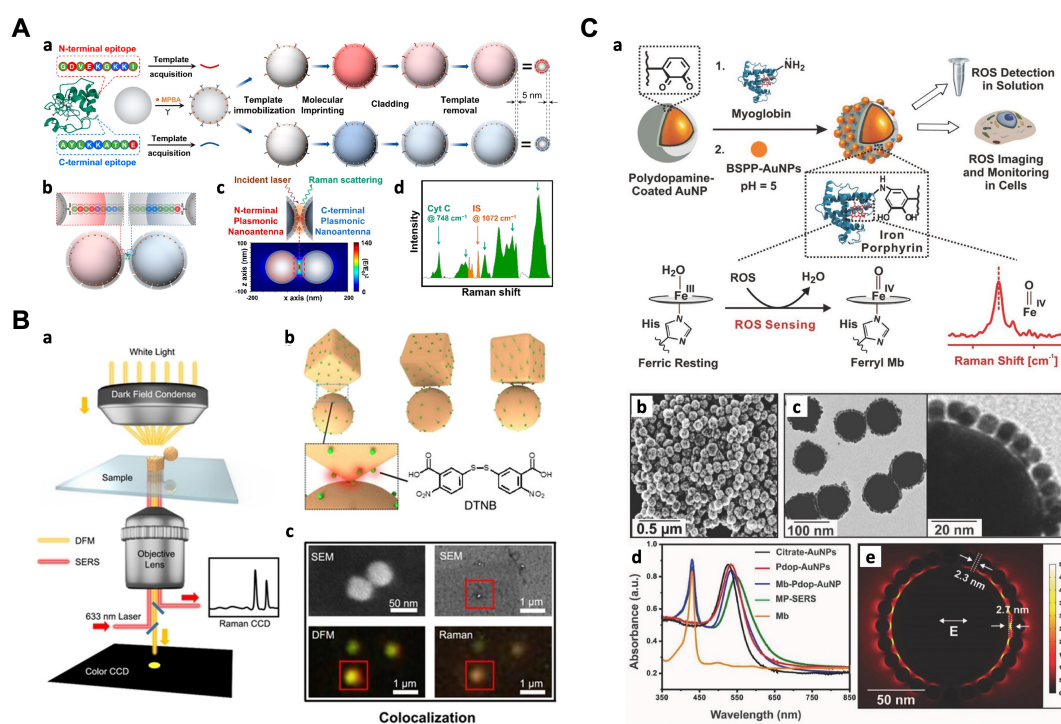


**Figure 3.** Representative substrates of coupled nanoparticles in colloidal suspension. (A) DBR-PNERS strategy for ultrasensitive protein fingerprinting and quantitation. (a) Preparation of terminal epitope-

imprinted PNAs; (b) protein-targeting DBR for fabrication of plasmonic nanogap; (c) protein-targeting EM enhancement for PNERs; (d) representative Raman spectrum for detection and molecular fingerprinting (reproduced with permission from Ref. [54], copyright 2022, American Chemical Society). (B) Single-particle SERS measurements of AANs with DTNB Raman dye on the surface. (a) Dark-field microscopy (DFM)-Raman integrated apparatus for measuring the structure-correlated optical and plasmonic properties of individual AANs; (b) schematic of AANs at different gap morphology with DTNB Raman dye on the surface; (c) the colocalization of scanning electron microscope (SEM), DFM characterization and Raman mapping of an on-vertex AAN (reproduced with permission from Ref. [55], copyright 2021, Wiley-VCH GmbH). (C) (a) Schematic representation for the synthesis of myoglobin and polydopamine-engineered SERS nanoprobe and SERS-based bio-detection chemistry of ROS at the porphyrin center of myoglobin; (b) SEM image of MP-SERS nanoprobe; (c) TEM images of MP-SERS nanoprobe; (d) UV-Vis spectra of citrate-AuNPs, pdop-AuNPs, Mb-functionalized pdop-AuNPs, MP-SERS nanoprobe, and Mb; (e) 3D-FEM simulation image of MP-SERS nanoprobe showing several hot spots (reproduced with permission from Ref. [56], copyright 2017, WILEY-VCH Verlag GmbH & Co. KGaA, Weinheim).

Recent progress in programmable materials has led to significant advancements in the field. Specifically, well-designed DNA nanostructures, including DNA origami, offer a highly programmable method for creating precise nanopatterns with nanoscale addressing capabilities [57,58]. This allows for the construction of architectures with precisely defined geometries [59–62]. Compared to nanoantenna gaps where molecules are adsorbed randomly on the surface, target molecules can be placed specifically in hotspots due to the nanogaps precisely controlled by self-assembled DNA nanostructures [63], providing single molecule resolution [64]. Even the anisotropic functionalization of plasmonic gold nanostructures with relative spatial directionality and sequence asymmetry is under precise control [65]. Moreover, the fabrication processes involved in DNA nanostructures are more cost-effective compared to traditional top-down lithographic techniques [66].

Taking advantage of these features, several SERS substrates have been developed with reliable signals. For example, Zhan et al. constructed plasmonic bowtie nanostructures using a DNA origami-based bottom-up assembly strategy, enabling precise control over the geometrical configuration of the bowtie with an approximate 5 nm gap [67]. A single Raman probe was accurately positioned at the gap of the bowtie, resulting in an exceptionally high enhancement factor of  $10^9$  so that a single-molecule level SERS detection is possible. Similarly, a DNA-based synthetic method for gold–silver core–shell nanodumbbells (GSNDs) was developed, offering good structural reproducibility and precise nanometer-level control over the size of the nanogaps across multiple particles [68]. The method involves preparing DNA-modified AuNPs by controlling the stoichiometric ratio of two thiolated DNA sequences. Each particle is modified with a maximum of one linking DNA strand, while densely modifying them with protecting DNA strands to maximize dimer yield and minimize higher multimeric structures. Subsequently, Ag nanoshells are formed on the Au dimers using polyvinylpyrrolidone (PVP)-based delivery of Ag precursors, enabling precise control and reproducibility of the interparticle gaps at the nanometer scale. Moreover, Niu et al. developed a DNA origami-based nanoprinting (DOBNP) strategy to transfer the essential DNA strands with predefined sequences and positions to the surface of AuNCs [55] (Figure 3B). This approach facilitated the controlled assembly of AuNC–AuNP nanostructures (AANs) with specific geometry and composition. The anchoring of a single dye molecule in hotspot regions results in a significant enhancement of the electromagnetic field, leading to a stronger amplification of the SERS signal.

Alternatively, nanoparticles of varying sizes or shapes can be assembled onto a central particle to form core-satellite assembled structures [56,69–72]. For instance, Kumar et al. developed myoglobin and polydopamine (pdop)-engineered SERS nanoprobe (MP-SERS) for real-time and quantitative detection of reactive oxygen species (ROS) levels in living cells [56] (Figure 3C). The probes consisted of 80 nm gold nanoparticles as a core, a thin

pdop layer as a spacer, Mb as a ROS-responsive Raman reporter, and 10 nm AuNPs as satellite particles. The plasmonic coupling between the core and satellites created a highly enhanced electromagnetic field in the interstitial sites, leading to nanogap-enhanced Raman scattering. The probes exhibited high sensitivity to ROS, good biocompatibility, and were successfully internalized into cells.

#### 4. Substrates on a Solid Support

Compared to traditional colloid-based systems, solid-supported SERS substrates offer numerous advantages. Nanostructures embedded on the surface exhibit high uniformity, provide compatibility with ultra-low volumes, enable single-nanoparticle measurements, and facilitate the preparation process. Similar to colloidal systems, various solid-supported substrates have been prepared. Colloidal nanoparticles, assemblies, or aggregates can be deposited onto surfaces [73–75]. A chemical layer can be used to functionalize surfaces and direct the adsorption of colloidal particles. [74,76]. By adjusting nanoparticle concentration and deposition time, the particle density on the surface can be optimized. These substrates offer similar advantages to colloidal systems while enabling comprehensive optical and structural characterization of individual particles during usage, which is particularly advantageous for single-molecule studies.

Apart from surface self-assembly methods, nanolithography is a commonly employed technique for fabricating surfaces with highly enhancing metal nanostructures. Colloidal lithography [77], and electron beam lithography (EBL) [78–80], are among the most prevalent lithographic methods used in SERS applications. These methods vary in terms of ease and cost of fabrication. Although lithography allows for the preparation of various highly sensitive structures, one drawback of deposited metal nanoparticles is their vulnerability to annealing, as structural changes in the nanoparticles can lead to shifts in LSPR position and alter SERS capabilities, sometimes even during the course of a measurement. Advancements in synthesis and nanolithography methods have contributed to higher field enhancements, improved spatial control, and greater uniformity and reproducibility.

##### 4.1. Bottom-Up Strategies

The bottom-up approach, mainly relying on self-assembly, offers a straightforward and high-throughput method for preparing SERS substrates. This approach involves organizing small nanoparticles into arrays with ordered nanostructures, and various techniques have been developed for this purpose. One method is oblique deposition, where nanoparticles are deposited at an angle to the substrate surface [81]. Another method is electro-displacement, which utilizes electrostatic forces to assemble nanoparticles into desired patterns [82].

Liquid substrate-based methods have gained popularity in bottom-up self-assembly in recent years. These methods allow for the formation of highly ordered nanostructures without complex instruments and additional materials. One example is the nanocapillary pumping model developed by Ge et al. [83]. In this model, a membrane structure with nanoparticles is subjected to solvent evaporation, then the surface of the film undergoes deformation, bringing the nanoparticles closer to each other and creating a substrate with hotspots in a large area. The pressure difference among gaps induces the movement of target molecules towards the smaller nanoparticle gaps, resulting in molecules trapped by the hotspots (Figure 4A). The detection limit is significantly reduced in this nanocapillary pump model. However, one limitation of this approach is the inability to control the nanoparticle array forming in a monolayer. Nanoparticles may obtain accumulated during the solvent evaporation, leading to plasmon resonance intensity of the substrate being non-uniform, reducing the reproducibility and reliability of SERS measurements. To address the challenges of non-uniform nanoparticle assembly and interference from non-adsorptive molecules in liquid SERS analysis, researchers have developed self-assembly methods depending on two-phase substrates and ternary regulations. In the two-phase substrate approach, gold nanoparticles tend to assemble at the interface of oil/water due to reduced electrostatic repulsion [84,85]. This leads to the formation of a large-scale self-assembled monolayer with controlled spacing on a nanometer

scale (Figure 4B). Such self-assembled monolayer provides a uniform distribution of hotspots, enhancing the performance of substrates. This method has been applied in various practical detection scenarios. For example, a liquid-like 3D plasmonic array was formed at the oil/water interface, enabling sensitive SERS analysis of different analytes [86]. The liquid interfacial plasmonic platform broke through the limitations of low molecular affinity and achieved sub-ppb level sensitivity. Researchers successfully detected polycyclic aromatic hydrocarbons and distinguished different molecular configurations using this approach.

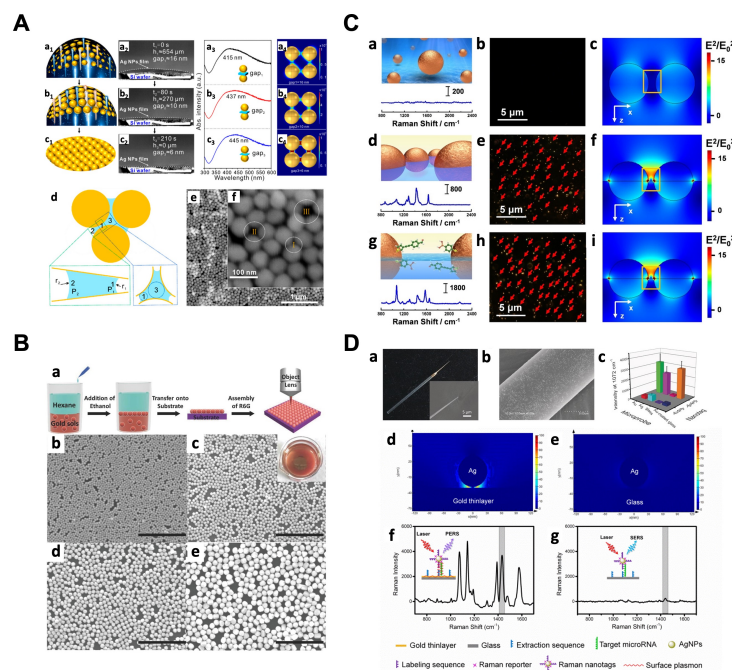


**Figure 4.** Representative substrates on a solid support using bottom-up strategies. (A) Formation of the nanocapillary pumping model; (a<sub>1</sub>–a<sub>4</sub>) schematic diagram of the assembled nanoparticle film, high-speed camera picture, in situ UV spectrum, and simulation of electromagnetic enhancement between nanoparticles with different gaps in the initial wet stage of the monolayer nanoparticle film; (b<sub>1</sub>–b<sub>4</sub>) formation of the effective hot-spot stage of the monolayer nanoparticle film; (c<sub>1</sub>–c<sub>4</sub>) final dry stage of the monolayer nanoparticle film; (d) principle causing the solvent to move toward the smaller gaps of the nanocapillary pumping model; (e,f) SEM image of the assembled monolayer silver nanoparticle film in the final dry stage (reproduced with permission from Ref. [83], copyright 2021, American Chemical Society). (B) (a) A scheme for fabricating and transferring Au nanoparticle monolayers from the water/hexane interface and an illustration of the SERS experiment; (b–e) SEM and optical images (inset) of the Au nanoparticle monolayer obtained through the water/oil interface by adjusting the addition of ethanol into different Au solutions with diameters of (b) 30 nm, (c) 60 nm, (d) 90 nm, and (e) 120 nm. Scale bar: 1 μm (reproduced with permission from Ref. [85], copyright 2016, WILEY-VCH Verlag GmbH & Co. KGaA, Weinheim). (C) Schematic and SERS spectrum of (a) AuNPs in water phase, (d) AuNPs at OA/W interface, and (g) AuNPs/RP1+MPBA at OA/W interface; (b,e,h) the corresponding dark field microscope image; (c,f,i) FDTD-calculated electromagnetic enhancement distribution for SERS in the xz-plane. The black dashed line indicates the OA/W interface (reproduced with permission from Ref. [87], copyright 2022, Wiley-VCH GmbH). (D) (a) Photo and SEM images of an extraction microprobe; (b) SEM image showing immunosandwiches formed on an extraction microprobe after extracting target protein from a single cell and being labeled with Raman nanotags; (c) dependence of Raman intensity on the combination of extraction microprobe and nanotag; electric-field intensity simulated by finite-difference time-domain (FDTD) under (d) PERS mode and (e) SERS mode; representative Raman spectra for (f) the PERS mode and (g) SERS mode, and insertions show the schematic of the principles of PERS and SERS modes (reproduced with permission from Ref. [88], copyright 2016, WILEY-VCH Verlag GmbH & Co. KGaA, Weinheim and under the terms of CC BY-NC 3.0 from Ref. [89], copyright 2018, the authors).

In the ternary regulation approach, charged noble metal nanoparticles are directly assembled under an electrostatic drive to form 2D thin arrays at the liquid/liquid interface [90]. The resulting nanoarray exhibits long-term stability and even distribution of hotspots. When transferred to a solid substrate, this nanoarray achieved single-cell Raman fingerprinting and discrimination of eight different bacteria species. However, controlling nanogaps at the molecular scale using interfacial tension and electrostatic forces can be challenging, leading to inaccuracies in trace substance analysis. Non-adsorptive molecules from complex biological systems may bring about interference in biological applications. To overcome these challenges, a novel interfacial SERS platform was developed using a functionalized AuNP array formed at the liquid/liquid interface [87]. This platform was achieved through ternary regulations involving double recognition of rigid molecular probes, uniform distribution of hotspots in a consistent manner, and the SERS readout in a silent region (Figure 4C). This platform allows real-time quantification, addressing signal interference and increasing the reliability of the SERS analysis. The reproducibility of the SERS analysis is improved by the fixed nanogap formed by the rigid structure of the probe. The use of specific Raman vibrations as signal output reduces interference from substances embedded in the brain.

A technique known as shell-isolated nanoparticle-enhanced Raman spectroscopy (SHINERS) has garnered significant attention and was introduced and developed by the Tian group [49,91]. In SHINERS, a thin dielectric layer is applied over the surface of metal nanoparticles, effectively creating a masking effect with a different material interface. This dielectric spacer layer, when sufficiently thin, allows molecules bound to the surface to experience a different surface chemistry while still benefiting from the significant field enhancement provided by the nearby metallic surface [92]. Silica is the most commonly used material for the shell in SHINERS, as it allows for the functionalization of gold and silver nanoparticles using silane chemistry, facilitating shell growth. This offers several advantages, including the ability to use different surface chemistry types for targeted adsorption in sensing applications, improved stability, and enhanced biocompatibility. Additionally, the use of insulating materials to create pinhole-free shells eliminates the occurrence of chemical enhancement resulting from charge transfer [49]. This altered interface between the shell and certain biological molecules or catalysts can lead to minimal perturbation of the electronic structure of the target caused by the underlying metal surface.

The Liu group developed a simple but effective approach named plasmon-enhanced Raman scattering (PERS) to provide ultrasensitive detection at the single-molecule level [88]. With the combination of gold substrate and silver nanoparticles, hotspots were generated with a 1–2 orders of magnitude higher signal compared to the conventional SERS mode with gold nanoparticles on a glass substrate (Figure 4D). Gold thin-layer-coated glass of a slightly lower enhancement was used as an alternative to save costs. AgNPs are uniformly dispersed on the Au layer, providing better reproducibility while maintaining high sensitivity compared with the coupling between particles. More importantly, the fabrication of substrates is simple and straight, which is conducive to the practical application. By the integration with microprobes for immunoaffinity extraction, a powerful tool for probing low-abundance proteins in single living cells has emerged. Depending on the interaction between the microprobe and the target, different bioassays, like the plasmonic immunosandwich assay (PISA) [88] and plasmonic affinity sandwich assay (PASA) [89], have been proposed and accomplished, empowering the analysis of low-abundance species, such as proteins and RNA in single cells.

#### 4.2. Top-Down Strategies

Top-down lithography techniques realize uniform hotspots on SERS substrates in a wide range with high precision. Electron beam lithography (EBL), a maskless technology that directly writes micro- and nanopatterns using an electron beam sensitive material, has shown compatibility with mass production manufacturing and excellent signal reproducibility [93,94]. For instance, on single-crystal Si substrates, nanopore arrays fabricated

using two-layer EBL demonstrated high sensitivity to the increased intensity of scattered light from enhanced incident electromagnetic radiation [95]. Focused ion beam (FIB) lithography, as another branch of top-down lithography, can focus the ion beams into tiny sizes using electrostatic lenses to achieve nanometer-scale positioning accuracy [96]. Etching techniques, which use physical or chemical methods to selectively remove unwanted moieties, enable high-throughput fabrication of substrates with desired nanostructures. Polymer nanopillars etched with Ar plasma from a polyethylene terephthalate (PET) substrate are subsequently deposited with Au, resulting in large-scale, highly reproducible SERS-active nanopillar arrays [97]. Chemical etching techniques can also be used to precisely regulate nanometer spacing. Porous nano-web structures fabricated by Lee et al. demonstrated a controllable gap between the nanoring core and the nano-web, confining the electromagnetic field in the nanogap [98]. The resulting structure demonstrated single-particle SERS dependent on the gap distance, being an ideal platform for SERS measurement for its structural integrity and stability, open accessibility of analytes, incident polarization independence, and reproducibility of SERS signals.

The combination of multiple nanofabrication technologies is emerging as a development trend in the SERS substrate preparation. Flauraud et al. utilized EBL and dry etching to fabricate lithographed funneled traps and auxiliary sidewalls on a solid substrate [99], directing the capillary assembly of Au nanorods, and achieving simultaneous control over their positions, orientations, and interparticle distances at the nanometer level. Multi-technique combination for biocompatible SERS-active materials is often used to enhance reliability. Li et al. fabricated digital nanopillar arrays with a combination of EBL, physical vapor deposition of Au, and selective reactive ion etching (RIE) to reveal the pillar structure [100] (Figure 5A). Four kinds of antibodies were conjugated to the array of pillars to selectively recognize cytokines, which were labeled with different Raman reporters to be visualized in color. The digital nanopillar SERS assay achieved highly specific and sensitive real-time cytokine detection down to the attomolar level, showing promise for advancing personalized medicine and predicting the higher risk of developing severe immune toxicities.

Colloidal lithography (also known as nanosphere lithography) involves monodispersed nanospheres as templates for the fabrication of SERS substrates in a wide range. By a chemical route, a colloidal template-induced precursor solution dipping strategy was used for the formation of periodic semi-hollow sphere arrays [101]. This array serves as a substrate for magnetron sputtering deposition of Au, resulting in novel micro/nanostructured arrays. These arrays offer diverse performance for different requirements. By involving a combination of molecular self-assembly, colloidal nanosphere lithography, and physical peeling, Luo et al. reported a fabrication process for fabricating large-area arrays of triangular nanogaps with adjustable widths ranging from ~10 to ~3 nm, exhibiting remarkably high measured enhancement factors of up to  $10^8$  compared to a thin gold film [102] (Figure 5B). Colloidal lithography can also form large-area nanostructures in parallel at low-cost on flexible substrates. An in situ chemical patterning technique is proposed based on plasmonic nanochemistry [103] (Figure 5C). A large-area-ordered Au nanohole array (NHA) film was prepared using colloidal lithography, where a polystyrene (PS) microsphere array was etched by the RIE process, and deposited with Au film. Via the wet chemical method, Ag nanoparticles were grown in situ from the edge to the center of the holes. After peeling off the Au NHA film, an ordered and large-area Ag nanoparticle assembly array (NAA) was left on the substrate. The region-specific Ag NAAs demonstrated outstanding SERS performance for quantitative detection and Raman imaging, with applications in multilevel encryption and anti-counterfeiting labels. This technique is also suitable for flexible substrates, such as polydimethylsiloxane (PDMS) and curved glass, allowing for extensive applications.

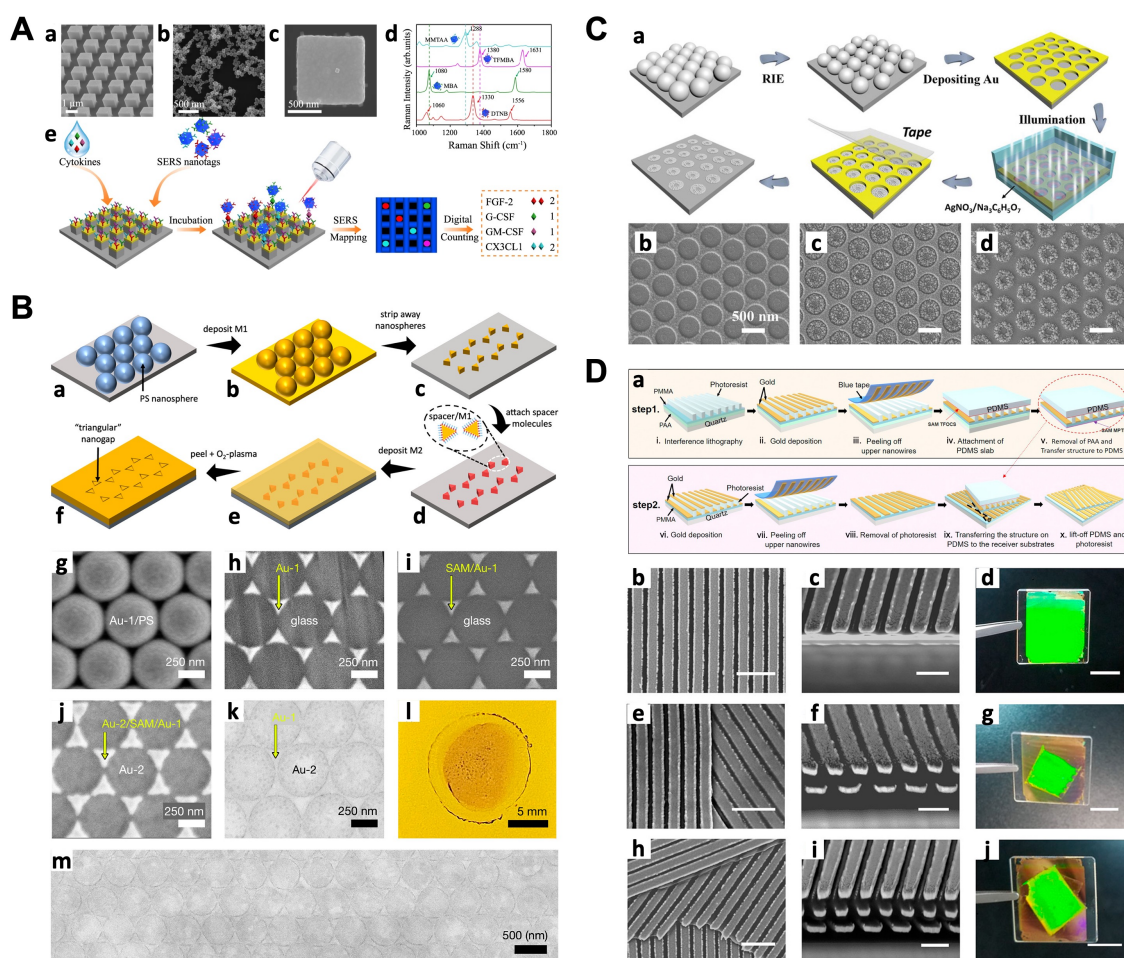


**Figure 5.** Representative substrates on a solid support using top-down strategies. (A) Digital single-molecule nanopillar SERS platform for parallel counting of four types of cytokines. SEM images of (a) pillar array side view, (b) nanoboxes, and (c) a single nanobox on the top of a pillar; (d) SERS spectra of nanoboxes conjugated with Raman reporters; (e) workflow for multiplex counting of cytokines (reproduced under the terms of CC BY 4.0 from Ref. [100], copyright 2021, the authors). (B) (a–f) Fabrication procedure for triangular nanogap arrays; (g–m) images of N = 1 Au/Au TNG arrays at various stages in the fabrication procedure (reproduced under the terms of CC BY 4.0 from Ref. [102], copyright 2022, the authors). (C) (a) Schematic of the fabrication process; SEM images of (b) Au NHAs, (c) Au NHAs with Ag NPs selectively growing in the interior of the holes, (d) Ag NP-NAAs after removing the NHA (reproduced with permission from Ref. [103], copyright 2021, Wiley-VCH GmbH). (D) (a) Schematics of the procedure for PAA-assisted nanotransfer printing to assemble 3D nanostructures layer-by-layer; (b–j) top- (b,e,h) and side-view (c,f,i) SEM images of the twisted triple-layer-grating nanostructures and their corresponding optical photographs (d,g,j); (b–d) the bottom nanograting layer; (e–g) double-layer 3D nanostructure with a twist angle  $\theta = 30^\circ$ ; (h–j) triple-layer 3D nanostructure with a twist angle between the neighboring nanogratings  $\theta = 30^\circ$ . Scale bar: 1  $\mu\text{m}$  (b,e,h), 500 nm (c,f,i), and 1 cm (d,g,j) (reproduced with permission from Ref. [104], copyright 2019, American Chemical Society).

In addition to traditional lithography methods, unconventional strategies, such as nanoprining, have been explored for the convenient fabrication of 3D nanostructures. Nanotransfer printing technology has been developed to transfer large-area and crack-free 3D multilayer nanostructures onto flexible substrates [104] (Figure 5D). This approach improves the uniformity and reproducibility of SERS substrates. Tape imprinting methods have been utilized to create lotus-shaped nanoarray structures with ultra-sensitive characteristics for detection [105]. Combination approaches, such as colloidal nanosphere

lithography with metal-assisted chemical etching, can produce nanopillar array SERS platforms with stable and reproducible Raman signals [106]. These platforms exhibit strong sensitivity and have applications in extended monitoring of cell surfaces and live cell analysis.

## 5. Applications

Conventional methods, such as bacterial culture, polymerase chain reaction (PCR), luminescence, and microarray are commonly utilized in the biomedical field to test clinical analytes. However, these methods have drawbacks including lengthy processing times, limited portability, insufficient multiplexing capabilities, and low sensitivity. In contrast, SERS provides rapid, on-site analysis with the ability to perform fingerprint multiplexing and achieve high sensitivity. Consequently, point-of-care (POC) SERS approaches have been developed and implemented to overcome the limitations of conventional methods. These approaches have been applied to various clinical samples, encompassing proteins, nucleic acids, and viruses.

### 5.1. Detection of Proteins

Protein biomarkers play a crucial role in disease diagnostics and treatment monitoring. The development of SERS-based bioassays for protein analysis has gained significant concern [107,108]. One approach is to incorporate SERS detection into lateral flow immunoassays (LFAs) using disposable and portable test strips [109–111]. In these SERS-LFA assays, ultrabright SERS nanotags conjugated with antibodies are used for sandwich recognition of the target protein in clinical samples. For example, a rapid SERS-LFA assay has been developed for the detection of human chorionic gonadotropin (hCG), a hormone associated with pregnancy [111]. This assay achieved fast detection within 2–5 seconds with a limit of detection (LOD) of approximately  $1.6 \text{ mIU} \cdot \text{mL}^{-1}$  using a portable Raman reader. Compared to traditional raster-scanning Raman microscopy, the use of line illumination significantly improved detection speed and sensitivity, making it 15 times more sensitive than commercial LFAs. In addition to SERS-LFA assays, the integration of digital microfluidics (DMF) with SERS-based immunoassays has been reported for protein detection [112] (Figure 6A). This approach involves a sandwich immunoassay in which magnetic beads coated with antibodies and antibody-functionalized SERS tags are used to capture and label the antigens for sensitive detection. The automation capability of DMF simplifies the assay procedure and minimizes the risk of exposure to hazardous samples.

The DMF-SERS method was utilized for the quantitative detection of H5N1, an avian influenza virus. This approach demonstrated outstanding sensitivity (LOD of  $74 \text{ pg} \cdot \text{mL}^{-1}$ ) and selectivity for H5N1 detection, with a shorter assay time ( $< 1 \text{ h}$ ) and reduced reagent consumption ( $\sim 30 \text{ } \mu\text{L}$ ) compared to the standard ELISA method. By combining DMF with a portable Raman spectrometer, this SERS offers a low reagent consumption and minimized exposure risk for hazardous samples, making it a promising tool for the diagnosis of infectious diseases.

Low-copy-number proteins that are expressed fewer than 1000 molecules per cell play vital roles in various essential cellular processes, yet accurately quantifying and understanding the functions of low-copy-number proteins at a single-cell level is challenging. Advanced techniques, such as the single-cell plasmonic immunosandwich assay (scPISA), are being developed to enhance the sensitivity and enable quantitative analysis of these proteins [113]. It combines *in vivo* microextraction for specific enrichment of target proteins from individual cells, and PERS for highly sensitive detection of low-copy-number proteins (Figure 6B). This approach holds great promise for advancing our understanding of cellular heterogeneity and the functions of low-copy-number proteins in biological processes and disease states [114,115]. PERS-based bioassays are not limited to a single-cell analysis. Depending on the principle of PERS, immunoassays that utilize antibodies or antibody mimics like molecular imprinting polymers (MIPs) and aptamers are effective in protein detection [116–120]. For example, Xing et al. presented an approach called the dual MIP-based

plasmonic immunosandwich assay (duMIP-PISA) for the sensitive and specific detection of protein biomarkers in complex biological samples [118]. By preparing a C-terminal epitope-imprinted self-assembled gold nanoparticle monolayer and N-terminal epitope-imprinted Raman-responsive Ag@SiO<sub>2</sub> nanoparticles, the target protein was specifically captured and labeled sequentially. The formation of the MIP-protein-MIP sandwich-like complexes results in a significantly enhanced SERS signal. The duMIP-PISA approach offers several advantages over regular enzyme-linked immunosorbent assay (ELISA), including a simpler procedure, faster speed, lower sample volume requirement, and wider linear range, making it a promising tool for various important applications, particularly in disease diagnosis.

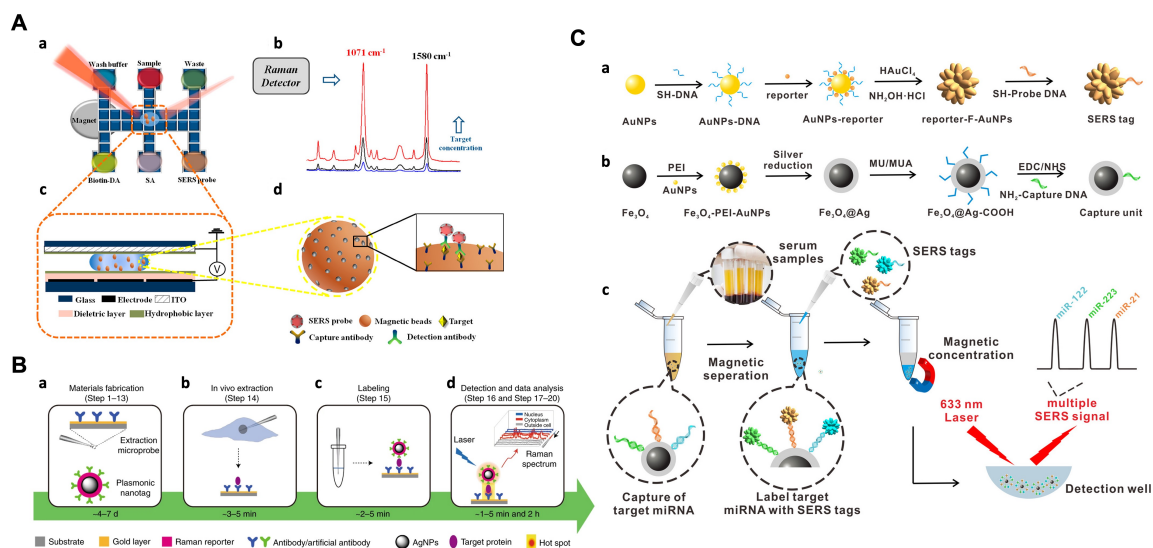


**Figure 6.** Representative applications of SERS bioassays for detection of proteins and nucleic acids. (A) Schematic illustration of SERS-based immunoassay with digital microfluidics. (a) Illustration of DMF-SERS method and bottom plate of DMF chip; (b) two characteristic Raman peaks of 4-MBA at 1071 and 1580 cm<sup>-1</sup>; (c) side view of DMF chip containing a droplet with magnetic beads; (d) immunocomplex functionalized with SERS tags on magnetic beads (reproduced with permission from Ref. [112], copyright 2018, American Chemical Society). (B) Overview of the scPISA procedure for the determination of low-copy-number proteins in single living cells. (a) Fabrication of the materials used for scPISA, including affinity ligand-functionalized gold-based extraction microprobe and affinity ligand-modified silver-based plasmonic nanotag; (b) in vivo extraction by an affinity extraction microprobe precisely inserted into a single living cell under test; (c) in vitro labeling of target protein captured from the single cell with plasmonic nanotag and the formation of extraction microprobe/protein/plasmonic nanotag sandwich-like immunocomplexes on the microprobe surface; (d) Raman signal readout by plasmonic detection and data analysis (reproduced with permission from Ref. [113], copyright 2021, the authors, under exclusive license to Springer Nature Limited). (C) Schematic illustration of multiplex miRNA assay via the SERS sandwich strategy. R6G-, CV-, and 4-ATP-encoded fractal Au nanoparticles were utilized as SERS tags, and Ag-coated magnetic nanoparticles were utilized as the capture substrate. (a) Schematic processes of synthesizing SERS tag; (b) design and synthesis of the capture substrate; (c) detection procedure of multiple miRNAs based on the capture substrate/miRNA/SERS tag sandwich structure (reproduced with permission from Ref. [121], copyright 2021, American Chemical Society).

## 5.2. Detection of Nucleic Acids

Nucleic acids, including RNA, DNA, and miRNA, play a crucial role as genetic material and serve as important biomarkers in various applications. Conventional methods for nucleic acid detection, such as real-time quantitative PCR (RT-qPCR) and northern blotting, often suffer from limitations such as low sensitivity, lack of portability, long assay times, and extensive sample preparations. To overcome these challenges, researchers have explored alternative detection methods, especially optical and electrochemical techniques.

Among these, SERS has become a promising strategy for nucleic acids, leading to the development of various SERS-based detection methods.

One particular class of nucleic acids, miRNA, consists of an average length of only 22 nucleotides. The short length and high sequence homology of miRNAs pose challenges for specific detection and amplification using conventional methods like PCR. However, miRNAs have raised potential as biomarkers of cancers since they play a critical role in protein post-transcriptional regulation. To address these limitations, many strategies based on SERS for miRNA detection have been proposed [121–127]. For example, a magnetically assisted sandwich-type SERS-based biosensor was manufactured [121], capable of ultrasensitive and multiplex detection of three hepatocellular carcinoma-related miRNA biomarkers (miRNA-122, miRNA-223, and miRNA-21) (Figure 6C). The biosensor consists of a magnetic capture substrate to capture DNA-conjugated Ag-coated magnetic nanoparticles (AgMNPs) and SERS tags to probe DNA-conjugated DNA-engineered fractal gold nanoparticles (F-AuNPs). This assay exhibited excellent selectivity, specificity, and high accuracy in multiplexed detection of actual human serum samples and liver cancer patient serum assay, even in the presence of other miRNAs. Remarkably, the LOD for the three miRNAs were exceptionally low, with values of 349 aM for miRNA-122, 374 aM for miRNA-223, and 311 aM for miRNA-21. Additionally, a technique named PASA was employed for the detection of nucleic acids [128] and their modifications [129] for several key advantages, including ultrahigh sensitivity, fast analysis time, and a minimal sample volume requirement. Zhang et al. developed a rapid and highly sensitive method called the AuNP-decorated Ag@SiO<sub>2</sub> nanocomposite-based PASA for the detection of circulating miRNAs in human serum [128]. Using this method, researchers successfully quantified miR-21 in human serum with a LOQ of 10<sup>-14</sup> M and differentiated a breast cancer patient from a healthy individual. The AuNP-decorated Ag@SiO<sub>2</sub> nanocomposite and PASA method can be easily adapted for the detection of other miRNAs and circulating tumor DNA, making it a promising tool for cancer diagnosis.

In addition to the detection of miRNA, longer nucleic acids, such as RNA and DNA, have also been successfully detected using SERS-based methods [130–138]. For example, a “lab-in-a-stick” portable device that integrates a SERS-based bioassay and the washing process has enabled the direct detection of pathogen RNA [133]. Two signal enhancement levels were utilized to achieve the sensitivity required for direct detection. Each target sequence was tagged with an ultrabright SERS-encoded nanorattle, providing ultrahigh SERS signals. These tagged target sequences were then concentrated into a focused spot for detection using hybridization sandwiches with magnetic microbeads. Through this approach, the device achieved direct detection of synthetic targets with a LOD of 200 fM. SERS devices have also been developed for the detection of DNA. DNA mutation pattern profiling is crucial for the classification of cancer types and plays a fundamental role in advancing precision medicine. Wu et al. developed an amplification-free SERS biochip that allows for the direct and simultaneous identification of multiple point mutations in tumor cells [135]. By integrating the SERS spectra encoding technique with a supervised learning algorithm, a panel of nucleotide mixtures can be effectively distinguished based on their mutation profiles. The SERS sensor is incorporated into a microfluidic chip, enabling one-step multiplex analysis within 40 min.

### 5.3. Detection of Viruses

The detection of viruses is crucial for early diagnosis and treatment and monitoring disease progression, especially in the context of recent pandemic and epidemic outbreaks like COVID-19. SERS-based detection methods for viruses have been developed, both in label-free and labeled approaches, offering rapid and reliable detection capabilities.

In label-free SERS detection, Yeh et al. presented a portable microfluidic platform named VIRRION (virus capture with rapid Raman spectroscopy detection and identification), which contains carbon nanotube arrays with differential filtration porosity, allowing for rapid enrichment and optical identification of viruses [139] (Figure 7A). The platform

employs a multi-virus capture component in conjunction with SERS, enabling real-time enrichment and identification of different emerging strains or unknown viruses. Following viral capture and detection on the chip, the viruses remain viable and become purified within the microdevice. This enables subsequent in-depth characterizations using various conventional methods. The technology successfully enriched and identified rhinovirus, influenza virus, and parainfluenza viruses, maintaining the stoichiometric viral proportions even when multiple types of viruses were present, simulating co-infection. The process of viral capture and detection took only a few minutes and resulted in a 70-fold enrichment enhancement, with a detection limit of  $10^2$  EID<sub>50</sub>·mL<sup>-1</sup> and a virus specificity of 90%, making it a promising tool for real-time tracking and monitoring of viral outbreaks.

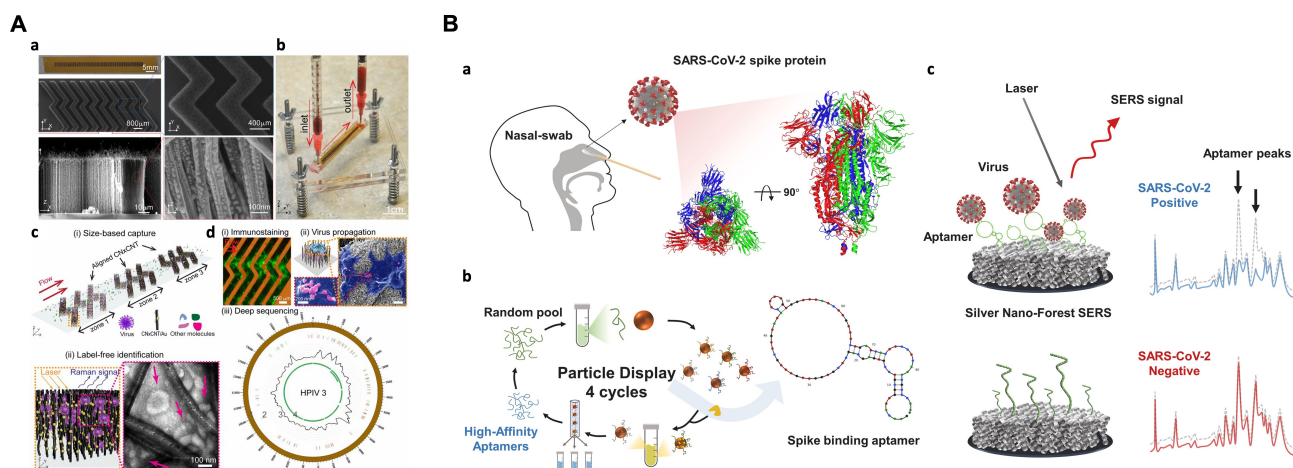


**Figure 7.** Representative applications of SERS bioassays for detection of viruses. **(A)** Design and working principle of VIRRION for effective virus capture and identification. **(a)** Photograph and SEM images of aligned CNTs exhibiting herringbone patterns decorated with gold nanoparticles; **(b)** picture showing assembled VIRRION device, processing a blood sample; **(c)** illustration of (i) size-based capture and (ii) in situ Raman spectroscopy for label-free optical virus identification; **(d)** on-chip virus analysis and enrichment for NGS, (i) on-chip immunostaining for captured H5N2, (ii) on-chip viral propagation through cell culture, and (iii) genomic sequencing and analysis of human parainfluenza virus type 3 (HPIV 3) (reproduced under the terms of CC BY 4.0 from Ref. [139], copyright 2020, the authors). **(B)** Design strategy for the label-free SERS-based aptasensor platform for SARS-CoV-2. **(a)** Targeted aptamer screening against spike (S) protein for detecting SARS-CoV-2 from clinical samples. Side and top view of the trimeric S protein on the surface of SARS-CoV-2 (PDB: 6VXX); **(b)** the particle display aptamer discovery process, in which solution-phase aptamer library molecules are converted to monoclonal aptamer particles, incubated with fluorescently-labeled S protein, and then subjected to fluorescence-activated cell sorting (FACS) to enrich library molecules with a strong affinity for this target; **(c)** the aptamer is then conjugated onto a silver nanoforest (SNF) substrate for the detection of SARS-CoV-2 and the intrinsic aptamer peaks shift in response to the conformational changes triggered by the S protein binding to the aptamer (reproduced with permission from Ref. [140], copyright 2023, Elsevier B.V.).

In the labeled SERS detection, typical immunoassays have been employed for virus detection [141–146]. For example, a highly sensitive and quantitative SERS-based LFA strip was developed for the simultaneous detection of influenza A H1N1 virus and human adenovirus (HAdV) [144]. Fe<sub>3</sub>O<sub>4</sub>@Ag nanoparticles served as magnetic SERS nanotags, which were conjugated with dual-layer Raman dye molecules and target virus-capture antibodies, allowing for specific recognition and magnetic enrichment of target viruses in the solution, as well as SERS detection of the viruses on the strip. The magnetic SERS strip can directly be used for real biological samples without requiring any sample pretreatment steps. The LOD achieved for H1N1 and HAdV were 50 and 10 pfu·mL<sup>-1</sup>, respectively, which were significantly higher compared to the standard colloidal gold strip method. This

SERS-based LFA strip is a potential tool for early detection of virus infections for its easy operation, rapidity, stability, and high throughput.

SERS also provides great potential for fast-screening detection of SARS-CoV-2 virus and its variants [140,147–153]. Park et al. developed an ultra-sensitive label-free aptasensor based on SERS for the universal detection of SARS-CoV-2 variants of concern [140] (Figure 7B). Two DNA aptamers with high affinity for binding to the spike protein of SARS-CoV-2 were first identified through high-throughput screening. The dissociation constants ( $k_D$ ) of the aptamers are  $1.47 \pm 0.30$  nM and  $1.81 \pm 0.39$  nM, respectively. By combining these aptamers with a silver nanoforest, this ultra-sensitive SERS platform achieves a detection limit at the attomolar ( $10^{-18}$  M) level using a recombinant trimeric spike protein. Furthermore, the intrinsic properties of the aptamer make the approach label-free, eliminating the need for a Raman tag. Clinical samples with variants of concern, like the wild-type, delta, and omicron variants, were successfully detected. In another study, a hand-held breathalyzer based on SERS for the rapid identification of individuals infected with COVID-19 was developed, which is capable of providing results in under 5 minutes and demonstrates high sensitivity (>95%) and specificity across a cohort of 501 participants [152]. These developments hold promise as a powerful tool for the rapid and reliable detection of SARS-CoV-2 variants, facilitating effective control measures against the ongoing pandemic.

While both label-free and labeled SERS bioassays have been developed for the detection of viruses, there is still a need for diverse functions, such as virus capture and enrichment, and minimized sample exposure, apart from sensitive, specific, and rapid detection. Such advancements would be highly desirable for real-world applications.

## 6. Conclusions and Future Perspectives

SERS has emerged as a very powerful and promising analytical technique, and its capabilities continue to advance primarily through improvements in substrates. The sensitivity, compatibility with probed molecules, and measurement reproducibility are determined by the substrate. These substrates often involve well-controlled particles and their tunable couplings to achieve optimal enhancement. While SERS-based bioassays have already been widely used in biomolecular detection, the rational design of substrates and applied methodologies discussed here will continue to drive advancements toward higher sensitivity and reproducibility for clinical applications. The labeled SERS bioassays using SERS nanotags for biomolecule detection offer a sensitive method with enhanced specificity through the use of targeting moieties on the nanoconstructs. One notable advantage of SERS nanotags is the ability to design and synthesize Raman-reporter labels with unique spectral peaks, enabling multiplex detection by avoiding overlap. These nanoprobe hold potential for early disease diagnosis, where simultaneous detection of multiple biomarkers at low concentrations is crucial.

Additionally, the implementation of artificial intelligence (AI) can greatly enhance the analysis of complex samples for which the involuted Raman spectra are often hard to distinguish, enabling disease diagnosis without the labeling of biomarkers [154–158]. For more related information, please refer to Ref. [159,160]. In brief, acquired Raman spectra in complex media can be processed using spectral unmixing algorithms to estimate concentration profiles, leading to improved quantification. By “learning” the fingerprint of Raman spectra and identifying specific characteristics from massive data, deep learning algorithms can automate analysis processes, outperforming human-operated analysis and potentially enabling more efficient and faster disease diagnosis. The combination of SERS signals with data processing software, especially involving AI, is an active area of research, offering potential improvements in accuracy and reliability.

While the SERS technique offers high sensitivity and intrinsic molecular fingerprint information, its reproducibility has historically been a challenge, limiting its widespread application. Recent advancements in nanotechnology have provided researchers with the means to create more uniform and reproducible SERS substrates, both at the mi-

cro/nanoscale and macroscopic levels. However, achieving precise nanogap regulation for specific recognition remains a critical requirement, especially in complex measurement environments. SERS analysis in vivo still pose both opportunities and challenges. One pressing need is to fix the nanogap between nanoparticles at a stable distance on a molecular level to achieve simultaneous reproducibility and selectivity in detection. Framework nucleic acids hold promise as they can integrate chemical recognition elements and provide a stable structure. By altering Raman reporters and refining molecule structures, it is possible to minimize fluctuations in the SERS signal. In addition, it is worth noting that some delicate methods, due to the complexity of their designs, may have a relatively high coefficient of variation in analyzing complex samples. Therefore, developing simple yet effective methods is of great importance for practical use in real-world applications.

Another significant challenge in advancing SERS is the limited availability of sensitive, affordable, and portable Raman spectrometers. Confocal Raman microscopy, despite its sensitivity, is often of cumbersome size and complex structure, limiting its usage as a portable device. Moreover, since only one micro area can be acquired at a time with Raman microscopy, bias may result from the microscopic heterogeneity, lacking representation at the overall level. To overcome this hurdle, extensive research is needed to develop miniaturized spectrometers with higher sensitive and Raman-stabilized lasers that can be seamlessly integrated into on-chip platforms. This development would be crucial in realizing the vision of portable and accessible SERS devices.

**Author Contributions:** Conceptualisation, S.G., Z.G. and Z.L.; writing—original draft preparation, S.G. and Z.L.; writing—review and editing, S.G., Z.G. and Z.L.; visualization, S.G.; supervision, Z.L.; funding acquisition, Z.L. All authors have read and agreed to the published version of the manuscript.

**Funding:** This research was funded by the Key Grant (21834003) and the Key Scientific Instrumentation Grant (21627810) from the National Natural Science Foundation of China.

**Institutional Review Board Statement:** Not applicable.

**Informed Consent Statement:** Not applicable.

**Data Availability Statement:** Data sharing not applicable.

**Conflicts of Interest:** The authors declare no conflict of interest.

## References

1. Raman, C.V.; Krishnan, K.S. A new type of secondary radiation. *Nature* **1928**, *121*, 501–502. [[CrossRef](#)]
2. Zong, C.; Xu, M.; Xu, L.J.; Wei, T.; Ma, X.; Zheng, X.S.; Hu, R.; Ren, B. Surface-enhanced Raman spectroscopy for bioanalysis: reliability and challenges. *Chem. Rev.* **2018**, *118*, 4946–4980. [[CrossRef](#)]
3. Howes, P.D.; Chandrawati, R.; Stevens, M.M. Colloidal nanoparticles as advanced biological sensors. *Science* **2014**, *346*, 1247390. [[CrossRef](#)] [[PubMed](#)]
4. Farka, Z.; Jurik, T.; Kovar, D.; Trnkova, L.; Skládal, P. Nanoparticle-based immunochemical biosensors and assays: Recent advances and challenges. *Chem. Rev.* **2017**, *117*, 9973–10042. [[CrossRef](#)]
5. Lane, L.A.; Qian, X.; Nie, S. SERS nanoparticles in medicine: from label-free detection to spectroscopic tagging. *Chem. Rev.* **2015**, *115*, 10489–10529. [[CrossRef](#)]
6. Kallaway, C.; Almond, L.M.; Barr, H.; Wood, J.; Hutchings, J.; Kendall, C.; Stone, N. Advances in the clinical application of Raman spectroscopy for cancer diagnostics. *Photodiagn. Photodyn. Ther.* **2013**, *10*, 207–219. [[CrossRef](#)] [[PubMed](#)]
7. Krafft, C.; Popp, J. The many facets of Raman spectroscopy for biomedical analysis. *Anal. Bioanal. Chem.* **2015**, *407*, 699–717. [[CrossRef](#)]
8. Stone, N.; Matousek, P. Advanced transmission Raman spectroscopy: A promising tool for breast disease diagnosis. *Cancer Res.* **2008**, *68*, 4424–4430. [[CrossRef](#)] [[PubMed](#)]
9. Movasaghi, Z.; Rehman, S.; Rehman, I.U. Raman spectroscopy of biological tissues. *Appl. Spectrosc. Rev.* **2007**, *42*, 493–541. [[CrossRef](#)]
10. Mosca, S.; Conti, C.; Stone, N.; Matousek, P. Spatially offset Raman spectroscopy. *Nat. Rev. Methods Primers* **2021**, *1*, 21. [[CrossRef](#)]
11. Ellis, D.I.; Cowcher, D.P.; Ashton, L.; O'Hagan, S.; Goodacre, R. Illuminating disease and enlightening biomedicine: Raman spectroscopy as a diagnostic tool. *Analyst* **2013**, *138*, 3871–3884. [[CrossRef](#)]
12. Fleischmann, M.; Hendra, P.J.; McQuillan, A.J. Raman spectra of pyridine adsorbed at a silver electrode. *Chem. Phys. Lett.* **1974**, *26*, 163–166. [[CrossRef](#)]

13. Jeanmaire, D.L.; Van Duyne, R.P. Surface Raman spectroelectrochemistry: Part I. Heterocyclic, aromatic, and aliphatic amines adsorbed on the anodized silver electrode. *J. Electroanal. Chem. Interfacial Electrochem.* **1977**, *84*, 1–20. [[CrossRef](#)]
14. Ye, J.; Chen, Y.; Liu, Z. A boronate affinity sandwich assay: an appealing alternative to immunoassays for the determination of glycoproteins. *Angew. Chem., Int. Ed.* **2014**, *53*, 10386–10389. [[CrossRef](#)]
15. Ahn, K.C.; Zhao, B.; Chen, J.; Cherednichenko, G.; Sanmarti, E.; Denison, M.S.; Lasley, B.; Pessah, I.N.; Kültz, D.; Chang, D.P.; et al. In vitro biologic activities of the antimicrobials triclocarban, its analogs, and triclosan in bioassay screens: receptor-based bioassay screens. *Environ. Health Perspect.* **2008**, *116*, 1203–1210. [[CrossRef](#)]
16. Fan, Y.; Wang, S.; Zhang, F. Optical Multiplexed Bioassays for Improved Biomedical Diagnostics. *Angew. Chem. Int. Ed.* **2019**, *58*, 13208–13219. [[CrossRef](#)] [[PubMed](#)]
17. Kerns, E.H.; Di, L.; Carter, G.T. In vitro solubility assays in drug discovery. *Curr. Drug Metab.* **2008**, *9*, 879–885. [[CrossRef](#)] [[PubMed](#)]
18. Johnson, I.; Hutchings, M.; Benstead, R.; Thain, J.; Whitehouse, P. Bioassay selection, experimental design and quality control/assurance for use in effluent assessment and control. *Ecotoxicology* **2004**, *13*, 437–447. [[CrossRef](#)]
19. Sprague, J. Measurement of pollutant toxicity to fish I. Bioassay methods for acute toxicity. *Water Res.* **1969**, *3*, 793–821. [[CrossRef](#)]
20. Schuetzle, D.; Lewtas, J. Bioassay-directed chemical analysis in environmental research. *Anal. Chem.* **1986**, *58*, 1060A–1075A. [[CrossRef](#)]
21. Rampersad, S.N. Multiple applications of Alamar Blue as an indicator of metabolic function and cellular health in cell viability bioassays. *Sensors* **2012**, *12*, 12347–12360. [[CrossRef](#)] [[PubMed](#)]
22. Laing, S.; Jamieson, L.E.; Faulds, K.; Graham, D. Surface-enhanced Raman spectroscopy for in vivo biosensing. *Nat. Rev. Chem.* **2017**, *1*, 0060. [[CrossRef](#)]
23. Francis, M.K.; Sahu, B.K.; Bhargav, P.B.; Balaji, C.; Ahmed, N.; Das, A.; Dhara, S. Ag nanowires based SERS substrates with very high enhancement factor. *Physica E Low Dimens. Syst. Nanostruct.* **2022**, *137*, 115080. [[CrossRef](#)]
24. Xu, S.; Man, B.; Jiang, S.; Wang, J.; Wei, J.; Xu, S.; Liu, H.; Gao, S.; Liu, H.; Li, Z.; et al. Graphene/Cu nanoparticle hybrids fabricated by chemical vapor deposition as surface-enhanced Raman scattering substrate for label-free detection of adenosine. *ACS Appl. Mater. Interfaces* **2015**, *7*, 10977–10987. [[CrossRef](#)] [[PubMed](#)]
25. Chen, S.; Li, X.; Zhao, Y.; Chang, L.; Qi, J. Graphene oxide shell-isolated Ag nanoparticles for surface-enhanced Raman scattering. *Carbon* **2015**, *81*, 767–772. [[CrossRef](#)]
26. Wang, X.; Huang, S.C.; Hu, S.; Yan, S.; Ren, B. Fundamental understanding and applications of plasmon-enhanced Raman spectroscopy. *Nat. Rev. Phys.* **2020**, *2*, 253–271. [[CrossRef](#)]
27. Langer, J.; Jimenez de Aberasturi, D.; Aizpurua, J.; Alvarez-Puebla, R.A.; Auguie, B.; Baumberg, J.J.; Bazan, G.C.; Bell, S.E.; Boisen, A.; Brolo, A.G.; et al. Present and future of surface-enhanced Raman scattering. *ACS Nano* **2019**, *14*, 28–117. [[CrossRef](#)]
28. Karthick Kannan, P.; Shankar, P.; Blackman, C.; Chung, C.H. Recent advances in 2D inorganic nanomaterials for SERS sensing. *Adv. Mater.* **2019**, *31*, 1803432. [[CrossRef](#)] [[PubMed](#)]
29. Shi, L.; Zhang, L.; Tian, Y. Rational Design of Surface-Enhanced Raman Scattering Substrate for Highly Reproducible Analysis. *Anal. Sens.* **2023**, *3*, e202200064. [[CrossRef](#)]
30. Lee, H.K.; Lee, Y.H.; Koh, C.S.L.; Phan-Quang, G.C.; Han, X.; Lay, C.L.; Sim, H.Y.F.; Kao, Y.C.; An, Q.; Ling, X.Y. Designing surface-enhanced Raman scattering (SERS) platforms beyond hotspot engineering: emerging opportunities in analyte manipulations and hybrid materials. *Chem. Soc. Rev.* **2019**, *48*, 731–756. [[CrossRef](#)]
31. Schlücker, S. Surface-Enhanced Raman Spectroscopy: Concepts and Chemical Applications. *Angew. Chem. Int. Ed.* **2014**, *53*, 4756–4795. [[CrossRef](#)]
32. Boujday, S.; Lamy de la Chapelle, M.; Srajer, J.; Knoll, W. Enhanced vibrational spectroscopies as tools for small molecule biosensing. *Sensors* **2015**, *15*, 21239–21264. [[CrossRef](#)]
33. Ding, H.; Hu, D.J.J.; Yu, X.; Liu, X.; Zhu, Y.; Wang, G. Review on all-fiber online Raman sensor with hollow core microstructured optical fiber. *Photonics* **2022**, *9*, 134. [[CrossRef](#)]
34. Jorgenson, E.; Ianoul, A. Biofunctionalization of plasmonic nanoparticles with short peptides monitored by SERS. *J. Phys. Chem. B* **2017**, *121*, 967–974. [[CrossRef](#)] [[PubMed](#)]
35. Chen, Y.; Xianyu, Y.; Jiang, X. Surface modification of gold nanoparticles with small molecules for biochemical analysis. *Acc. Chem. Res.* **2017**, *50*, 310–319. [[CrossRef](#)]
36. He, J.; Unser, S.; Bruzas, I.; Cary, R.; Shi, Z.; Mehra, R.; Aron, K.; Sagle, L. The facile removal of CTAB from the surface of gold nanorods. *Colloids Surf.* **2018**, *163*, 140–145. [[CrossRef](#)] [[PubMed](#)]
37. Zheng, Y.; Zhong, X.; Li, Z.; Xia, Y. Successive, Seed-Mediated Growth for the Synthesis of Single-Crystal Gold Nanospheres with Uniform Diameters Controlled in the Range of 5–150 nm. *Part. Part. Syst. Charact.* **2014**, *31*, 266–273. [[CrossRef](#)]
38. Niu, W.; Chua, Y.A.A.; Zhang, W.; Huang, H.; Lu, X. Highly symmetric gold nanostars: crystallographic control and surface-enhanced Raman scattering property. *J. Am. Chem. Soc.* **2015**, *137*, 10460–10463. [[CrossRef](#)]
39. Khoury, C.G.; Vo-Dinh, T. Gold nanostars for surface-enhanced Raman scattering: synthesis, characterization and optimization. *J. Phys. Chem. C* **2008**, *112*, 18849–18859. [[CrossRef](#)] [[PubMed](#)]
40. Childs, A.; Vinogradova, E.; Ruiz-Zepeda, F.; Velazquez-Salazar, J.J.; Jose-Yacamán, M. Biocompatible gold/silver nanostars for surface-enhanced Raman scattering. *J. Raman Spectrosc.* **2016**, *47*, 651–655. [[CrossRef](#)]

41. Scarabelli, L.; Liz-Marzan, L.M. An extended protocol for the synthesis of monodisperse gold nanotriangles. *ACS Nano* **2021**, *15*, 18600–18607. [[CrossRef](#)]
42. Khanal, B.P.; Zubarev, E.R. Chemical transformation of nanorods to nanowires: Reversible growth and dissolution of anisotropic gold nanostructures. *ACS Nano* **2019**, *13*, 2370–2378. [[CrossRef](#)] [[PubMed](#)]
43. González-Rubio, G.; Díaz-Núñez, P.; Rivera, A.; Prada, A.; Tardajos, G.; González-Izquierdo, J.; Bañares, L.; Llombart, P.; Macdowell, L.G.; Alcolea Palafox, M.; et al. Femtosecond laser reshaping yields gold nanorods with ultranarrow surface plasmon resonances. *Science* **2017**, *358*, 640–644. [[CrossRef](#)] [[PubMed](#)]
44. Deng, R.; Qu, H.; Liang, L.; Zhang, J.; Zhang, B.; Huang, D.; Xu, S.; Liang, C.; Xu, W. Tracing the therapeutic process of targeted aptamer/drug conjugate on cancer cells by surface-enhanced Raman scattering spectroscopy. *Anal. Chem.* **2017**, *89*, 2844–2851. [[CrossRef](#)] [[PubMed](#)]
45. Park, J.E.; Lee, Y.; Nam, J.M. Precisely shaped, uniformly formed gold nanocubes with ultrahigh reproducibility in single-particle scattering and surface-enhanced Raman scattering. *Nano Lett.* **2018**, *18*, 6475–6482. [[CrossRef](#)]
46. Matteini, P.; Cottat, M.; Tavanti, F.; Panfilova, E.; Scuderi, M.; Nicotra, G.; Menziani, M.C.; Khlebtsov, N.; de Angelis, M.; Pini, R. Site-selective surface-enhanced Raman detection of proteins. *ACS Nano* **2017**, *11*, 918–926. [[CrossRef](#)]
47. Guo, P.; Sikdar, D.; Huang, X.; Si, K.J.; Xiong, W.; Gong, S.; Yap, L.W.; Premaratne, M.; Cheng, W. Plasmonic core-shell nanoparticles for SERS detection of the pesticide thiram: size-and shape-dependent Raman enhancement. *Nanoscale* **2015**, *7*, 2862–2868. [[CrossRef](#)]
48. Jana, D.; Gorunmez, Z.; He, J.; Bruzas, I.; Beck, T.; Sagle, L. Surface enhanced Raman spectroscopy of a Au@Au core-shell structure containing a spiky shell. *J. Phys. Chem. C* **2016**, *120*, 20814–20821. [[CrossRef](#)]
49. Li, J.F.; Zhang, Y.J.; Ding, S.Y.; Panneerselvam, R.; Tian, Z.Q. Core-shell nanoparticle-enhanced Raman spectroscopy. *Chem. Rev.* **2017**, *117*, 5002–5069. [[CrossRef](#)]
50. Zhang, P.; Li, Y.; Wang, D.; Xia, H. High-Yield Production of Uniform Gold Nanoparticles with Sizes from 31 to 577 nm via One-Pot Seeded Growth and Size-Dependent SERS Property. *Part. Part. Syst. Charact.* **2016**, *33*, 924–932. [[CrossRef](#)]
51. Zhang, D.; Tang, L.; Chen, J.; Tang, Z.; Liang, P.; Huang, Y.; Cao, M.; Zou, M.; Ni, D.; Chen, J.; et al. Controllable self-assembly of SERS hotspots in liquid environment. *Langmuir* **2021**, *37*, 939–948. [[CrossRef](#)] [[PubMed](#)]
52. Shin, J.; Lee, S.; Yoo, S.; Jung, I.; Lee, S.; Kim, J.; Son, J.; Kim, J.E.; Kim, J.M.; Nam, J.M.; et al. Enormous enhancement in single-particle surface-enhanced Raman scattering with size-controllable Au double nanorings. *Chem. Mater.* **2022**, *34*, 2197–2205. [[CrossRef](#)]
53. Cho, N.H.; Byun, G.H.; Lim, Y.C.; Im, S.W.; Kim, H.; Lee, H.E.; Ahn, H.Y.; Nam, K.T. Uniform chiral gap synthesis for high dissymmetry factor in single plasmonic gold nanoparticle. *ACS Nano* **2020**, *14*, 3595–3602. [[CrossRef](#)] [[PubMed](#)]
54. He, H.; Zhou, L.; Guo, Z.; Li, P.; Gao, S.; Liu, Z. Dual Biomimetic Recognition-Driven Plasmonic Nanogap-Enhanced Raman Scattering for Ultrasensitive Protein Fingerprinting and Quantitation. *Nano Lett.* **2022**, *22*, 9664–9671. [[CrossRef](#)] [[PubMed](#)]
55. Niu, R.; Song, C.; Gao, F.; Fang, W.; Jiang, X.; Ren, S.; Zhu, D.; Su, S.; Chao, J.; Chen, S.; et al. DNA Origami-Based Nanoprinting for the Assembly of Plasmonic Nanostructures with Single-Molecule Surface-Enhanced Raman Scattering. *Angew. Chem. Int. Ed.* **2021**, *60*, 11695–11701. [[CrossRef](#)] [[PubMed](#)]
56. Kumar, S.; Kumar, A.; Kim, G.H.; Rhim, W.K.; Hartman, K.L.; Nam, J.M. Myoglobin and polydopamine-engineered Raman nanoprobes for detecting, imaging, and monitoring reactive oxygen species in biological samples and living cells. *Small* **2017**, *13*, 1701584. [[CrossRef](#)] [[PubMed](#)]
57. Hong, F.; Zhang, F.; Liu, Y.; Yan, H. DNA origami: scaffolds for creating higher order structures. *Chem. Rev.* **2017**, *117*, 12584–12640. [[CrossRef](#)]
58. Liu, N.; Liedl, T. DNA-assembled advanced plasmonic architectures. *Chem. Rev.* **2018**, *118*, 3032–3053. [[CrossRef](#)]
59. Liu, W.; Halverson, J.; Tian, Y.; Tkachenko, A.V.; Gang, O. Self-organized architectures from assorted DNA-framed nanoparticles. *Nat. Chem.* **2016**, *8*, 867–873. [[CrossRef](#)]
60. Liu, Z.; Pei, H.; Zhang, L.; Tian, Y. Mitochondria-targeted DNA nanoprobe for real-time imaging and simultaneous quantification of Ca<sup>2+</sup> and pH in neurons. *ACS Nano* **2018**, *12*, 12357–12368. [[CrossRef](#)]
61. Huang, X.; Zhao, W.; Chen, X.; Li, J.; Ye, H.; Li, C.; Yin, X.; Zhou, X.; Qiao, X.; Xue, Z.; et al. Gold nanoparticle-bridge array to improve DNA hybridization efficiency of SERS sensors. *J. Am. Chem. Soc.* **2022**, *144*, 17533–17539. [[CrossRef](#)] [[PubMed](#)]
62. Niu, R.; Gao, F.; Wang, D.; Zhu, D.; Su, S.; Chen, S.; YuWen, L.; Fan, C.; Wang, L.; Chao, J. Pattern recognition directed assembly of Plasmonic gap nanostructures for single-molecule SERS. *ACS Nano* **2022**, *16*, 14622–14631. [[CrossRef](#)]
63. Fang, W.; Jia, S.; Chao, J.; Wang, L.; Duan, X.; Liu, H.; Li, Q.; Zuo, X.; Wang, L.; Wang, L.; et al. Quantizing single-molecule surface-enhanced Raman scattering with DNA origami metamolecules. *Sci. Adv.* **2019**, *5*, eaau4506. [[CrossRef](#)] [[PubMed](#)]
64. Simoncelli, S.; Roller, E.M.; Urban, P.; Schreiber, R.; Turberfield, A.J.; Liedl, T.; Lohmuller, T. Quantitative single-molecule surface-enhanced Raman scattering by optothermal tuning of DNA origami-assembled plasmonic nanoantennas. *ACS Nano* **2016**, *10*, 9809–9815. [[CrossRef](#)] [[PubMed](#)]
65. Liu, B.; Song, C.; Zhu, D.; Wang, X.; Zhao, M.; Yang, Y.; Zhang, Y.; Su, S.; Shi, J.; Chao, J.; et al. DNA-Origami-based assembly of anisotropic plasmonic gold nanostructures. *Small* **2017**, *13*, 1603991. [[CrossRef](#)] [[PubMed](#)]
66. Tanwar, S.; Haldar, K.K.; Sen, T. DNA origami directed Au nanostar dimers for single-molecule surface-enhanced Raman scattering. *J. Am. Chem. Soc.* **2017**, *139*, 17639–17648. [[CrossRef](#)]

67. Zhan, P.; Wen, T.; Wang, Z.g.; He, Y.; Shi, J.; Wang, T.; Liu, X.; Lu, G.; Ding, B. DNA origami directed assembly of gold bowtie nanoantennas for single-molecule surface-enhanced Raman scattering. *Angew. Chem. Int. Ed.* **2018**, *57*, 2846–2850. [[CrossRef](#)]
68. Lim, D.K.; Jeon, K.S.; Kim, H.M.; Nam, J.M.; Suh, Y.D. Nanogap-engineerable Raman-active nanodumbbells for single-molecule detection. *Nat. Mater.* **2010**, *9*, 60–67. [[CrossRef](#)]
69. Gandra, N.; Abbas, A.; Tian, L.; Singamaneni, S. Plasmonic planet–satellite analogues: hierarchical self-assembly of gold nanostructures. *Nano Lett.* **2012**, *12*, 2645–2651. [[CrossRef](#)]
70. Li, A.; Tang, L.; Song, D.; Song, S.; Ma, W.; Xu, L.; Kuang, H.; Wu, X.; Liu, L.; Chen, X.; et al. A SERS-active sensor based on heterogeneous gold nanostar core–silver nanoparticle satellite assemblies for ultrasensitive detection of aflatoxinB1. *Nanoscale* **2016**, *8*, 1873–1878. [[CrossRef](#)]
71. Li, Q.; Ge, X.; Ye, J.; Li, Z.; Su, L.; Wu, Y.; Yang, H.; Song, J. Dual ratiometric SERS and photoacoustic core–satellite nanoprobe for quantitatively visualizing hydrogen peroxide in inflammation and cancer. *Angew. Chem. Int. Ed.* **2021**, *60*, 7323–7332. [[CrossRef](#)] [[PubMed](#)]
72. Hu, C.; Hu, Y.; Fan, C.; Yang, L.; Zhang, Y.; Li, H.; Xie, W. Surface-enhanced Raman spectroscopic evidence of key intermediate species and role of NiFe dual-catalytic center in water oxidation. *Angew. Chem. Int. Ed.* **2021**, *60*, 19774–19778. [[CrossRef](#)] [[PubMed](#)]
73. Rodríguez-Lorenzo, L.; Alvarez-Puebla, R.A.; Pastoriza-Santos, I.; Mazzucco, S.; Stéphan, O.; Kociak, M.; Liz-Marzán, L.M.; García de Abajo, F.J. Zeptomol detection through controlled ultrasensitive surface-enhanced Raman scattering. *J. Am. Chem. Soc.* **2009**, *131*, 4616–4618. [[CrossRef](#)] [[PubMed](#)]
74. Su, Q.; Ma, X.; Dong, J.; Jiang, C.; Qian, W. A reproducible SERS substrate based on electrostatically assisted APTES-functionalized surface-assembly of gold nanostars. *ACS Appl. Mater. Interfaces* **2011**, *3*, 1873–1879. [[CrossRef](#)] [[PubMed](#)]
75. Fortuni, B.; Fujita, Y.; Ricci, M.; Inose, T.; Aubert, R.; Lu, G.; Hutchison, J.A.; Hofkens, J.; Latterini, L.; Uji-i, H. A novel method for in situ synthesis of SERS-active gold nanostars on polydimethylsiloxane film. *Chem. Commun.* **2017**, *53*, 5121–5124. [[CrossRef](#)]
76. Lee, J.; Hua, B.; Park, S.; Ha, M.; Lee, Y.; Fan, Z.; Ko, H. Tailoring surface plasmons of high-density gold nanostar assemblies on metal films for surface-enhanced Raman spectroscopy. *Nanoscale* **2014**, *6*, 616–623. [[CrossRef](#)] [[PubMed](#)]
77. Zrimsek, A.B.; Henry, A.I.; Van Duyne, R.P. Single molecule surface-enhanced Raman spectroscopy without nanogaps. *J. Phys. Chem. Lett.* **2013**, *4*, 3206–3210. [[CrossRef](#)]
78. Das, G.; Chirumamilla, M.; Toma, A.; Gopalakrishnan, A.; Zaccaria, R.P.; Alabastri, A.; Leoncini, M.; Di Fabrizio, E. Plasmon based biosensor for distinguishing different peptides mutation states. *Sci. Rep.* **2013**, *3*, 1792. [[CrossRef](#)]
79. Chirumamilla, M.; Toma, A.; Gopalakrishnan, A.; Das, G.; Zaccaria, R.P.; Krahne, R.; Rondanina, E.; Leoncini, M.; Liberale, C.; De Angelis, F.; et al. 3D nanostar dimers with a sub-10-nm gap for single-/few-molecule surface-enhanced Raman scattering. *Adv. Mater.* **2014**, *26*, 2353–2358. [[CrossRef](#)]
80. Gopalakrishnan, A.; Chirumamilla, M.; De Angelis, F.; Toma, A.; Zaccaria, R.P.; Krahne, R. Bimetallic 3D nanostar dimers in ring cavities: recyclable and robust surface-enhanced Raman scattering substrates for signal detection from few molecules. *ACS Nano* **2014**, *8*, 7986–7994. [[CrossRef](#)]
81. Liu, Y.; Wu, H.; Ma, L.; Zou, S.; Ling, Y.; Zhang, Z. Highly stable and active SERS substrates with Ag–Ti alloy nanorods. *Nanoscale* **2018**, *10*, 19863–19870. [[CrossRef](#)] [[PubMed](#)]
82. Han, W.; Stepula, E.; Philippi, M.; Schlücker, S.; Steinhart, M. Evaluation of 3D gold nanodendrite layers obtained by templated galvanic displacement reactions for SERS sensing and heterogeneous catalysis. *Nanoscale* **2018**, *10*, 20671–20680. [[CrossRef](#)] [[PubMed](#)]
83. Ge, M.; Li, P.; Zhou, G.; Chen, S.; Han, W.; Qin, F.; Nie, Y.; Wang, Y.; Qin, M.; Huang, G.; et al. General surface-enhanced Raman spectroscopy method for actively capturing target molecules in small gaps. *J. Am. Chem. Soc.* **2021**, *143*, 7769–7776. [[CrossRef](#)] [[PubMed](#)]
84. Kim, K.; Han, H.S.; Choi, I.; Lee, C.; Hong, S.; Suh, S.H.; Lee, L.P.; Kang, T. Interfacial liquid-state surface-enhanced Raman spectroscopy. *Nat. Commun.* **2013**, *4*, 2182. [[CrossRef](#)] [[PubMed](#)]
85. Si, S.; Liang, W.; Sun, Y.; Huang, J.; Ma, W.; Liang, Z.; Bao, Q.; Jiang, L. Facile fabrication of high-density sub-1-nm gaps from Au nanoparticle monolayers as reproducible SERS substrates. *Adv. Funct. Mater.* **2016**, *26*, 8137–8145. [[CrossRef](#)]
86. Tian, L.; Su, M.; Yu, F.; Xu, Y.; Li, X.; Li, L.; Liu, H.; Tan, W. Liquid-state quantitative SERS analyzer on self-ordered metal liquid-like plasmonic arrays. *Nat. Commun.* **2018**, *9*, 3642. [[CrossRef](#)] [[PubMed](#)]
87. Shi, L.; Liu, M.; Zhang, L.; Tian, Y. A liquid interfacial SERS platform on a nanoparticle array stabilized by rigid probes for the quantification of norepinephrine in rat brain microdialysates. *Angew. Chem. Int. Ed.* **2022**, *61*, e202117125.
88. Liu, J.; Yin, D.; Wang, S.; Chen, H.Y.; Liu, Z. Probing Low-Copy-Number Proteins in a Single Living Cell. *Angew. Chem. Int. Ed.* **2016**, *55*, 13215–13218. [[CrossRef](#)]
89. Liu, J.; Wen, Y.; He, H.; Chen, H.Y.; Liu, Z. Probing cytoplasmic and nuclear microRNAs in single living cells via plasmonic affinity sandwich assay. *Chem. Sci.* **2018**, *9*, 7241–7246. [[CrossRef](#)]
90. Tian, T.; Yi, J.; Liu, Y.; Li, B.; Liu, Y.; Qiao, L.; Zhang, K.; Liu, B. Self-assembled plasmonic nanoarrays for enhanced bacterial identification and discrimination. *Biosens. Bioelectron.* **2022**, *197*, 113778. [[CrossRef](#)]
91. Li, J.F.; Huang, Y.F.; Ding, Y.; Yang, Z.L.; Li, S.B.; Zhou, X.S.; Fan, F.R.; Zhang, W.; Zhou, Z.Y.; Wu, D.Y.; et al. Shell-isolated nanoparticle-enhanced Raman spectroscopy. *Nature* **2010**, *464*, 392–395. [[CrossRef](#)] [[PubMed](#)]

92. Tian, X.D.; Liu, B.J.; Li, J.F.; Yang, Z.L.; Ren, B.; Tian, Z.Q. SHINERS and plasmonic properties of Au Core SiO<sub>2</sub> shell nanoparticles with optimal core size and shell thickness. *J. Raman Spectrosc.* **2013**, *44*, 994–998. [[CrossRef](#)]
93. Duan, H.; Hu, H.; Kumar, K.; Shen, Z.; Yang, J.K. Direct and reliable patterning of plasmonic nanostructures with sub-10-nm gaps. *ACS Nano* **2011**, *5*, 7593–7600. [[CrossRef](#)] [[PubMed](#)]
94. Tu, M.; Xia, B.; Kravchenko, D.E.; Tietze, M.L.; Cruz, A.J.; Stassen, I.; Hauffman, T.; Teyssandier, J.; De Feyter, S.; Wang, Z.; et al. Direct X-ray and electron-beam lithography of halogenated zeolitic imidazolate frameworks. *Nat. Mater.* **2021**, *20*, 93–99. [[CrossRef](#)] [[PubMed](#)]
95. Scherrer, D.; Vogel, D.; Drechsler, U.; Olziersky, A.; Sparr, C.; Mayor, M.; Lörtscher, E. Monitoring Solid-Phase Reactions in Self-Assembled Monolayers by Surface-Enhanced Raman Spectroscopy. *Angew. Chem. Int. Ed.* **2021**, *60*, 17981–17988. [[CrossRef](#)]
96. Schröder, T.; Trusheim, M.E.; Walsh, M.; Li, L.; Zheng, J.; Schukraft, M.; Sipahigil, A.; Evans, R.E.; Sukachev, D.D.; Nguyen, C.T.; et al. Scalable focused ion beam creation of nearly lifetime-limited single quantum emitters in diamond nanostructures. *Nat. Commun.* **2017**, *8*, 15376. [[CrossRef](#)] [[PubMed](#)]
97. Park, S.G.; Xiao, X.; Min, J.; Mun, C.; Jung, H.S.; Giannini, V.; Weissleder, R.; Maier, S.A.; Im, H.; Kim, D.H. Self-assembly of nanoparticle-spiked pillar arrays for plasmonic biosensing. *Adv. Funct. Mater.* **2019**, *29*, 1904257. [[CrossRef](#)]
98. Lee, S.; Lee, S.; Son, J.; Kim, J.M.; Lee, J.; Yoo, S.; Haddadnezhad, M.; Shin, J.; Kim, J.; Nam, J.M.; et al. Web-above-a-Ring (WAR) and Web-above-a-Lens (WAL): Nanostructures for Highly Engineered Plasmonic-Field Tuning and SERS Enhancement. *Small* **2021**, *17*, 2101262. [[CrossRef](#)]
99. Flauraud, V.; Mastrangeli, M.; Bernasconi, G.D.; Butet, J.; Alexander, D.T.; Shahrabi, E.; Martin, O.J.; Brugger, J. Nanoscale topographical control of capillary assembly of nanoparticles. *Nat. Nanotechnol.* **2017**, *12*, 73–80. [[CrossRef](#)]
100. Li, J.; Wuethrich, A.; Sina, A.A.; Cheng, H.H.; Wang, Y.; Behren, A.; Mainwaring, P.N.; Trau, M. A digital single-molecule nanopillar SERS platform for predicting and monitoring immune toxicities in immunotherapy. *Nat. Commun.* **2021**, *12*, 1087. [[CrossRef](#)]
101. Zhang, H.; Liu, M.; Zhou, F.; Liu, D.; Liu, G.; Duan, G.; Cai, W.; Li, Y. Physical deposition improved SERS stability of morphology controlled periodic micro/nanostructured arrays based on colloidal templates. *Small* **2015**, *11*, 844–853. [[CrossRef](#)]
102. Luo, S.; Mancini, A.; Wang, F.; Liu, J.; Maier, S.A.; de Mello, J.C. High-throughput fabrication of triangular nanogap arrays for surface-enhanced Raman spectroscopy. *ACS Nano* **2022**, *16*, 7438–7447. [[CrossRef](#)] [[PubMed](#)]
103. Guan, Y.; Ai, B.; Wang, Z.; Chen, C.; Zhang, W.; Wang, Y.; Zhang, G. In situ chemical patterning technique. *Adv. Funct. Mater.* **2022**, *32*, 2107945. [[CrossRef](#)]
104. Zheng, C.; Shen, Y.; Liu, M.; Liu, W.; Wu, S.; Jin, C. Layer-by-layer assembly of three-dimensional optical functional nanostructures. *ACS Nano* **2019**, *13*, 5583–5590. [[CrossRef](#)] [[PubMed](#)]
105. Wang, Y.; Zhang, M.; Feng, L.; Dong, B.; Xu, T.; Li, D.; Jiang, L.; Chi, L. Tape-imprinted hierarchical lotus seedpod-like arrays for extraordinary surface-enhanced Raman spectroscopy. *Small* **2019**, *15*, 1804527. [[CrossRef](#)] [[PubMed](#)]
106. Lin, D.; Wu, Z.; Li, S.; Zhao, W.; Ma, C.; Wang, J.; Jiang, Z.; Zhong, Z.; Zheng, Y.; Yang, X. Large-area Au-nanoparticle-functionalized Si nanorod arrays for spatially uniform surface-enhanced Raman spectroscopy. *ACS Nano* **2017**, *11*, 1478–1487. [[CrossRef](#)]
107. Kamil Reza, K.; Wang, J.; Vaidyanathan, R.; Dey, S.; Wang, Y.; Trau, M. Electrohydrodynamic-induced SERS immunoassay for extensive multiplexed biomarker sensing. *Small* **2017**, *13*, 1602902. [[CrossRef](#)]
108. Lai, Y.; Schlücker, S.; Wang, Y. Rapid and sensitive SERS detection of the cytokine tumor necrosis factor alpha (tnf- $\alpha$ ) in a magnetic bead pull-down assay with purified and highly Raman-active gold nanoparticle clusters. *Anal. Bioanal. Chem.* **2018**, *410*, 5993–6000. [[CrossRef](#)]
109. Sánchez-Purrà, M.; Carré-Camps, M.; de Puig, H.; Bosch, I.; Gehrke, L.; Hamad-Schifferli, K. Surface-enhanced Raman spectroscopy-based sandwich immunoassays for multiplexed detection of Zika and Dengue viral biomarkers. *ACS Infect. Dis.* **2017**, *3*, 767–776. [[CrossRef](#)]
110. Hu, S.W.; Qiao, S.; Pan, J.B.; Kang, B.; Xu, J.J.; Chen, H.Y. A paper-based SERS test strip for quantitative detection of Mucin-1 in whole blood. *Talanta* **2018**, *179*, 9–14. [[CrossRef](#)]
111. Tran, V.; Walkenfort, B.; König, M.; Salehi, M.; Schlücker, S. Rapid, quantitative, and ultrasensitive point-of-care testing: A portable SERS reader for lateral flow assays in clinical chemistry. *Angew. Chem. Int. Ed.* **2019**, *58*, 442–446. [[CrossRef](#)] [[PubMed](#)]
112. Wang, Y.; Ruan, Q.; Lei, Z.C.; Lin, S.C.; Zhu, Z.; Zhou, L.; Yang, C. Highly sensitive and automated surface enhanced Raman scattering-based immunoassay for H5N1 detection with digital microfluidics. *Anal. Chem.* **2018**, *90*, 5224–5231. [[CrossRef](#)]
113. Liu, J.; He, H.; Xie, D.; Wen, Y.; Liu, Z. Probing low-copy-number proteins in single living cells using single-cell plasmonic immunosandwich assays. *Nat. Protoc.* **2021**, *16*, 3522–3546. [[CrossRef](#)] [[PubMed](#)]
114. Xie, D.; Wen, Y.; Chen, J.; Guo, Z.; Li, P.; Liu, Z. Probing Protein 4'-Phosphopantetheinylation in Single Living Cells. *Anal. Chem.* **2023**, *95*, 7229–7236. [[CrossRef](#)] [[PubMed](#)]
115. Wen, Y.; Zhao, J.; He, H.; Zhao, Q.; Liu, Z. Multiplexed single-cell plasmonic immunoassay of intracellular signaling proteins enables non-destructive monitoring of cell fate. *Anal. Chem.* **2021**, *93*, 14204–14213. [[CrossRef](#)] [[PubMed](#)]
116. Muhammad, P.; Tu, X.; Liu, J.; Wang, Y.; Liu, Z. Molecularly imprinted plasmonic substrates for specific and ultrasensitive immunoassay of trace glycoproteins in biological samples. *ACS Appl. Mater. Interfaces* **2017**, *9*, 12082–12091. [[CrossRef](#)] [[PubMed](#)]

117. Zhou, L.; Wang, Y.; Xing, R.; Chen, J.; Liu, J.; Li, W.; Liu, Z. Orthogonal dual molecularly imprinted polymer-based plasmonic immunosandwich assay: a double characteristic recognition strategy for specific detection of glycoproteins. *Biosens. Bioelectron.* **2019**, *145*, 111729. [[CrossRef](#)]
118. Xing, R.; Wen, Y.; Dong, Y.; Wang, Y.; Zhang, Q.; Liu, Z. Dual molecularly imprinted polymer-based plasmonic immunosandwich assay for the specific and sensitive detection of protein biomarkers. *Anal. Chem.* **2019**, *91*, 9993–10000. [[CrossRef](#)]
119. Pang, J.; Li, P.; He, H.; Xu, S.; Liu, Z. Molecularly imprinted polymers outperform lectin counterparts and enable more precise cancer diagnosis. *Chem. Sci.* **2022**, *13*, 4589–4597. [[CrossRef](#)]
120. Guo, Z.; Zhang, Q.; Xing, R.; Liu, Z. Molecularly imprinted and cladded polymers for constructing a portable plasmonic immunoassay for peptides in biofluids. *Chem. Commun.* **2023**, *59*, 3075–3078. [[CrossRef](#)]
121. Wu, J.; Zhou, X.; Li, P.; Lin, X.; Wang, J.; Hu, Z.; Zhang, P.; Chen, D.; Cai, H.; Niessner, R.; et al. Ultrasensitive and simultaneous SERS detection of multiplex microRNA using fractal gold nanotags for early diagnosis and prognosis of hepatocellular carcinoma. *Anal. Chem.* **2021**, *93*, 8799–8809. [[CrossRef](#)] [[PubMed](#)]
122. Zhou, W.; Tian, Y.F.; Yin, B.C.; Ye, B.C. Simultaneous surface-enhanced Raman spectroscopy detection of multiplexed microRNA biomarkers. *Anal. Chem.* **2017**, *89*, 6120–6128. [[CrossRef](#)] [[PubMed](#)]
123. Ma, D.; Huang, C.; Zheng, J.; Tang, J.; Li, J.; Yang, J.; Yang, R. Quantitative detection of exosomal microRNA extracted from human blood based on surface-enhanced Raman scattering. *Biosens. Bioelectron.* **2018**, *101*, 167–173. [[CrossRef](#)] [[PubMed](#)]
124. Lee, J.U.; Kim, W.H.; Lee, H.S.; Park, K.H.; Sim, S.J. Quantitative and specific detection of exosomal miRNAs for accurate diagnosis of breast cancer using a surface-enhanced Raman scattering sensor based on plasmonic head-flocked gold nanopillars. *Small* **2019**, *15*, 1804968. [[CrossRef](#)] [[PubMed](#)]
125. Pang, Y.; Wang, C.; Lu, L.; Wang, C.; Sun, Z.; Xiao, R. Dual-SERS biosensor for one-step detection of microRNAs in exosome and residual plasma of blood samples for diagnosing pancreatic cancer. *Biosens. Bioelectron.* **2019**, *130*, 204–213. [[CrossRef](#)] [[PubMed](#)]
126. Jiang, S.; Li, Q.; Wang, C.; Pang, Y.; Sun, Z.; Xiao, R. In situ exosomal MicroRNA determination by target-triggered SERS and Fe<sub>3</sub>O<sub>4</sub>@TiO<sub>2</sub>-based exosome accumulation. *ACS Sens.* **2021**, *6*, 852–862. [[CrossRef](#)] [[PubMed](#)]
127. Zhou, H.; Zhang, J.; Li, B.; Liu, J.; Xu, J.J.; Chen, H.Y. Dual-mode SERS and electrochemical detection of miRNA based on popcorn-like gold nanofilms and toehold-mediated strand displacement amplification reaction. *Anal. Chem.* **2021**, *93*, 6120–6127. [[CrossRef](#)]
128. Zhang, Q.; Liu, J.; Dong, Y.; Li, W.; Xing, R.; Ma, Y.; Liu, Z. Gold nanoparticle-decorated Ag@SiO<sub>2</sub> nanocomposite-based plasmonic affinity sandwich assay of circulating microRNAs in human serum. *ACS Appl. Nano Mater.* **2019**, *2*, 3960–3970. [[CrossRef](#)]
129. Xie, D.; Wen, Y.; Chen, J.; Lu, H.; He, H.; Liu, Z. Probing Queuosine Modifications of Transfer RNA in Single Living Cells via Plasmonic Affinity Sandwich Assay. *Anal. Chem.* **2022**, *94*, 12828–12835. [[CrossRef](#)]
130. Zhou, Q.; Zheng, J.; Qing, Z.; Zheng, M.; Yang, J.; Yang, S.; Ying, L.; Yang, R. Detection of circulating tumor DNA in human blood via DNA-mediated surface-enhanced Raman spectroscopy of single-walled carbon nanotubes. *Anal. Chem.* **2016**, *88*, 4759–4765. [[CrossRef](#)]
131. Fu, X.; Cheng, Z.; Yu, J.; Choo, P.; Chen, L.; Choo, J. A SERS-based lateral flow assay biosensor for highly sensitive detection of HIV-1 DNA. *Biosens. Bioelectron.* **2016**, *78*, 530–537. [[CrossRef](#)]
132. Wu, L.; Xiao, X.; Chen, K.; Yin, W.; Li, Q.; Wang, P.; Lu, Z.; Ma, J.; Han, H. Ultrasensitive SERS detection of *Bacillus thuringiensis* special gene based on Au@Ag NRs and magnetic beads. *Biosens. Bioelectron.* **2017**, *92*, 321–327. [[CrossRef](#)] [[PubMed](#)]
133. Ngo, H.T.; Freedman, E.; Odion, R.A.; Strobbia, P.; De Silva Indrasekara, A.S.; Vohra, P.; Taylor, S.M.; Vo-Dinh, T. Direct detection of unamplified pathogen RNA in blood lysate using an integrated lab-in-a-stick device and ultrabright SERS nanorattles. *Sci. Rep.* **2018**, *8*, 4075. [[CrossRef](#)]
134. Zhang, Y.; Wang, Z.; Wu, L.; Zong, S.; Yun, B.; Cui, Y. Combining multiplex SERS nanovectors and multivariate analysis for in situ profiling of circulating tumor cell phenotype using a microfluidic chip. *Small* **2018**, *14*, 1704433. [[CrossRef](#)] [[PubMed](#)]
135. Wu, L.; Teixeira, A.; Garrido-Maestu, A.; Muinelo-Romay, L.; Lima, L.; Santos, L.L.; Prado, M.; Diéguez, L. Profiling DNA mutation patterns by SERS fingerprinting for supervised cancer classification. *Biosens. Bioelectron.* **2020**, *165*, 112392. [[CrossRef](#)] [[PubMed](#)]
136. Liu, Y.; Lyu, N.; Rajendran, V.K.; Piper, J.; Rodger, A.; Wang, Y. Sensitive and direct DNA mutation detection by surface-enhanced Raman spectroscopy using rational designed and tunable plasmonic nanostructures. *Anal. Chem.* **2020**, *92*, 5708–5716. [[CrossRef](#)] [[PubMed](#)]
137. Moitra, P.; Chaichi, A.; Hasan, S.M.A.; Dighe, K.; Alafeef, M.; Prasad, A.; Gartia, M.R.; Pan, D. Probing the mutation independent interaction of DNA probes with SARS-CoV-2 variants through a combination of surface-enhanced Raman scattering and machine learning. *Biosens. Bioelectron.* **2022**, *208*, 114200. [[CrossRef](#)] [[PubMed](#)]
138. Choi, J.H.; Shin, M.; Yang, L.; Conley, B.; Yoon, J.; Lee, S.N.; Lee, K.B.; Choi, J.W. Clustered regularly interspaced short palindromic repeats-mediated amplification-free detection of viral DNAs using surface-enhanced Raman spectroscopy-active nanoarray. *ACS Nano* **2021**, *15*, 13475–13485. [[CrossRef](#)]
139. Yeh, Y.T.; Gulino, K.; Zhang, Y.; Sabestien, A.; Chou, T.W.; Zhou, B.; Lin, Z.; Albert, I.; Lu, H.; Swaminathan, V.; et al. A rapid and label-free platform for virus capture and identification from clinical samples. *Proc. Natl. Acad. Sci. USA* **2020**, *117*, 895–901. [[CrossRef](#)]

140. Park, K.S.; Choi, A.; Kim, H.J.; Park, I.; Eom, M.S.; Yeo, S.G.; Son, R.G.; Park, T.I.; Lee, G.; Soh, H.T.; et al. Ultra-sensitive label-free SERS biosensor with high-throughput screened DNA aptamer for universal detection of SARS-CoV-2 variants from clinical samples. *Biosens. Bioelectron.* **2023**, *228*, 115202. [[CrossRef](#)]
141. Kamińska, A.; Witkowska, E.; Winkler, K.; Dzieciulewski, I.; Weyher, J.L.; Waluk, J. Detection of Hepatitis B virus antigen from human blood: SERS immunoassay in a microfluidic system. *Biosens. Bioelectron.* **2015**, *66*, 461–467. [[CrossRef](#)] [[PubMed](#)]
142. Sun, Y.; Xu, L.; Zhang, F.; Song, Z.; Hu, Y.; Ji, Y.; Shen, J.; Li, B.; Lu, H.; Yang, H. A promising magnetic SERS immunosensor for sensitive detection of avian influenza virus. *Biosens. Bioelectron.* **2017**, *89*, 906–912. [[CrossRef](#)] [[PubMed](#)]
143. Camacho, S.A.; Sobral-Filho, R.G.; Aoki, P.H.B.; Constantino, C.J.L.; Brolo, A.G. Zika immunoassay based on surface-enhanced Raman scattering nanoprobe. *ACS Sens.* **2018**, *3*, 587–594. [[CrossRef](#)] [[PubMed](#)]
144. Wang, C.; Wang, C.; Wang, X.; Wang, K.; Zhu, Y.; Rong, Z.; Wang, W.; Xiao, R.; Wang, S. Magnetic SERS strip for sensitive and simultaneous detection of respiratory viruses. *ACS Appl. Mater. Interfaces* **2019**, *11*, 19495–19505. [[CrossRef](#)] [[PubMed](#)]
145. Chen, H.; Park, S.G.; Choi, N.; Moon, J.I.; Dang, H.; Das, A.; Lee, S.; Kim, D.G.; Chen, L.; Choo, J. SERS imaging-based aptasensor for ultrasensitive and reproducible detection of influenza virus A. *Biosens. Bioelectron.* **2020**, *167*, 112496. [[CrossRef](#)] [[PubMed](#)]
146. Zhuang, J.; Zhao, Z.; Lian, K.; Yin, L.; Wang, J.; Man, S.; Liu, G.; Ma, L. SERS-based CRISPR/Cas assay on microfluidic paper analytical devices for supersensitive detection of pathogenic bacteria in foods. *Biosens. Bioelectron.* **2022**, *207*, 114167. [[CrossRef](#)] [[PubMed](#)]
147. Yadav, S.; Sadique, M.A.; Ranjan, P.; Kumar, N.; Singhal, A.; Srivastava, A.K.; Khan, R. SERS based lateral flow immunoassay for point-of-care detection of SARS-CoV-2 in clinical samples. *ACS Appl. Bio Mater.* **2021**, *4*, 2974–2995. [[CrossRef](#)]
148. Sitjar, J.; Liao, J.D.; Lee, H.; Tsai, H.P.; Wang, J.R.; Liu, P.Y. Challenges of SERS technology as a non-nucleic acid or-antigen detection method for SARS-CoV-2 virus and its variants. *Biosens. Bioelectron.* **2021**, *181*, 113153. [[CrossRef](#)]
149. Liu, H.; Dai, E.; Xiao, R.; Zhou, Z.; Zhang, M.; Bai, Z.; Shao, Y.; Qi, K.; Tu, J.; Wang, C.; et al. Development of a SERS-based lateral flow immunoassay for rapid and ultra-sensitive detection of anti-SARS-CoV-2 IgM/IgG in clinical samples. *Sens. Actuators B* **2021**, *329*, 129196. [[CrossRef](#)]
150. Zhang, M.; Li, X.; Pan, J.; Zhang, Y.; Zhang, L.; Wang, C.; Yan, X.; Liu, X.; Lu, G. Ultrasensitive detection of SARS-CoV-2 spike protein in untreated saliva using SERS-based biosensor. *Biosens. Bioelectron.* **2021**, *190*, 113421. [[CrossRef](#)]
151. Chen, H.; Park, S.G.; Choi, N.; Kwon, H.J.; Kang, T.; Lee, M.K.; Choo, J. Sensitive detection of SARS-CoV-2 using a SERS-based aptasensor. *ACS Sens.* **2021**, *6*, 2378–2385. [[CrossRef](#)] [[PubMed](#)]
152. Leong, S.X.; Leong, Y.X.; Tan, E.X.; Sim, H.Y.F.; Koh, C.S.L.; Lee, Y.H.; Chong, C.; Ng, L.S.; Chen, J.R.T.; Pang, D.W.C.; et al. Noninvasive and point-of-care surface-enhanced Raman scattering (SERS)-based breathalyzer for mass screening of coronavirus disease 2019 (COVID-19) under 5 min. *ACS Nano* **2022**, *16*, 2629–2639. [[CrossRef](#)]
153. Peng, Y.; Lin, C.; Li, Y.; Gao, Y.; Wang, J.; He, J.; Huang, Z.; Liu, J.; Luo, X.; Yang, Y. Identifying infectiousness of SARS-CoV-2 by ultra-sensitive SnS<sub>2</sub> SERS biosensors with capillary effect. *Matter* **2022**, *5*, 694–709. [[CrossRef](#)] [[PubMed](#)]
154. Shin, H.; Oh, S.; Hong, S.; Kang, M.; Kang, D.; Ji, Y.g.; Choi, B.H.; Kang, K.W.; Jeong, H.; Park, Y.; et al. Early-stage lung cancer diagnosis by deep learning-based spectroscopic analysis of circulating exosomes. *ACS Nano* **2020**, *14*, 5435–5444. [[CrossRef](#)] [[PubMed](#)]
155. Huang, Z.; Siddhanta, S.; Zheng, G.; Kickler, T.; Barman, I. Rapid, Label-free Optical Spectroscopy Platform for Diagnosis of Heparin-Induced Thrombocytopenia. *Angew. Chem. Int. Ed.* **2020**, *59*, 5972–5978. [[CrossRef](#)] [[PubMed](#)]
156. Xie, Y.; Su, X.; Wen, Y.; Zheng, C.; Li, M. Artificial intelligent label-free SERS profiling of serum exosomes for breast cancer diagnosis and postoperative assessment. *Nano Lett.* **2022**, *22*, 7910–7918. [[CrossRef](#)]
157. Shu, W.; Zhang, M.; Zhang, C.; Li, R.; Pei, C.; Zeng, Y.; Zhao, L.; Zhao, J.; Wan, J. An Alloy Platform of Dual-Fingerprints for High-Performance Stroke Screening. *Adv. Funct. Mater.* **2023**, *33*, 2210267. [[CrossRef](#)]
158. Huang, L.; Sun, H.; Sun, L.; Shi, K.; Chen, Y.; Ren, X.; Ge, Y.; Jiang, D.; Liu, X.; Knoll, W.; et al. Rapid, label-free histopathological diagnosis of liver cancer based on Raman spectroscopy and deep learning. *Nat. Commun.* **2023**, *14*, 48. [[CrossRef](#)]
159. Lussier, F.; Thibault, V.; Charron, B.; Wallace, G.Q.; Masson, J.F. Deep learning and artificial intelligence methods for Raman and surface-enhanced Raman scattering. *TrAC Trends Anal. Chem.* **2020**, *124*, 115796. [[CrossRef](#)]
160. Luo, R.; Popp, J.; Bocklitz, T. Deep learning for Raman spectroscopy: A review. *Analytica* **2022**, *3*, 287–301. [[CrossRef](#)]

**Disclaimer/Publisher’s Note:** The statements, opinions and data contained in all publications are solely those of the individual author(s) and contributor(s) and not of MDPI and/or the editor(s). MDPI and/or the editor(s) disclaim responsibility for any injury to people or property resulting from any ideas, methods, instructions or products referred to in the content.